P-98

IDENTIFICATION OF LINEARIZED EQUATIONS OF MOTION FOR THE FIXED WING CONFIGURATION OF THE ROTOR SYSTEMS RESEARCH AIRCRAFT

FINAL REPORT

PRINCIPAL INVESTIGATORS

Dwight L. Balough

Doral R. Sandlin

03/19/85-03/19/86

California Polytechnic State University

Aeronautical Engineering Department

San Luis Obispo, California

Grant No. NCC2-258

ABSTRACT

IDENTIFICATION OF LINEARIZED EQUATIONS OF MOTION FOR THE FIXED WING CONFIGURATION OF THE ROTOR SYSTEMS RESEARCH AIRCRAFT

Dwight L. Balough

March 1986

The purpose of this report is to establish linear, decoupled models of rigid body motion for the fixed wing configuration of the Rotor Systems Research Aircraft. Longitudinal and lateral control surface fixed linear models were created from aircraft time histories using current system identification techniques. Models were obtained from computer simulation at 160 KCAS and 200 KCAS, and from flight data at 160 KCAS. Comparisons were performed to examine modeling accuracy, variation of dynamics with airspeed and correlation of simulation and flight data results. The results showed that the longitudinal and lateral linear models accurately predicted RSRA dynamics. The flight data results showed that no significant handling qualities problems were present in the RSRA fixed wing aircraft at the flight speed tested.

Table of Contents

Tables

Table Page

Figures

Symbols

CG: aircraft center of gravity

F: matrix containing identified force and moment coefficients

G: matrix containing identified control coefficients

KCAS: calibrated airspeed in knots

L,M,N: body axes aerodynamic moments about CG

p,q,r: body axes angular velocity components about CG

P,Q,R: body axes angular velocities at trim condition

R^2: multiple correlation coefficient

$t_{1/2}$: time to damp to half amplitude

t_2: time to double amplitude

w_n: undamped natural frequency

u(t): vector of control surface inputs

u,v,w: body axes velocity components of CG

U,V,W: body axes velocities at trim condition

x(t): vector of longitudinal or lateral state variables

α_W: wing angle of attack

δ_{AIL}: aileron deflection

δ_{HT}: horizontal tail deflection

δ_{RUD}: rudder deflection

δ_{XB}: longitudinal stick deflection

θ, ϕ: aircraft attitude and bank angles respectively

$\bar{\theta}$, $\bar{\Phi}$: trim values of aircraft attitude and bank angles respectively

z: damping ratio

CHAPTER 1

Introduction

The Rotor Systems Research Aircraft (RSRA) is a flight research vehicle dedicated to the experimental investigation of rotor systems concepts. The RSRA is a unique aircraft, combining the principles of both fixed wing and rotary wing flight in an effort to better understand the complicated aerodynamics of the rotor system. The RSRA aircraft, as shown in Figure 1, can be flown in three basic configurations: the fixed wing mode, the compound mode, and the pure helicopter mode. The RSRA compound configuration consists of both a helicopter rotary wing system and a variable incidence fixed airfoil. By changing the incidence of the airfoil, the amount of lift created by the fixed wing system can be varied. This in turn alters the load carried by the rotary wing system. This ability to load or unload the rotor system was the primary reason for the addition of the variable incidence wing. Since the RSRA utilizes new and experimental rotor systems, the fixed wing mode was also desirable for safety of flight reasons. That is, in the case of a rotor system malfunction, the RSRA can jettison the main rotor blades through a series of explosive charges, and fly safely in the fixed wing mode.

Because the aircraft had never flown in the fixed wing configuration, a series of flight tests was conducted at

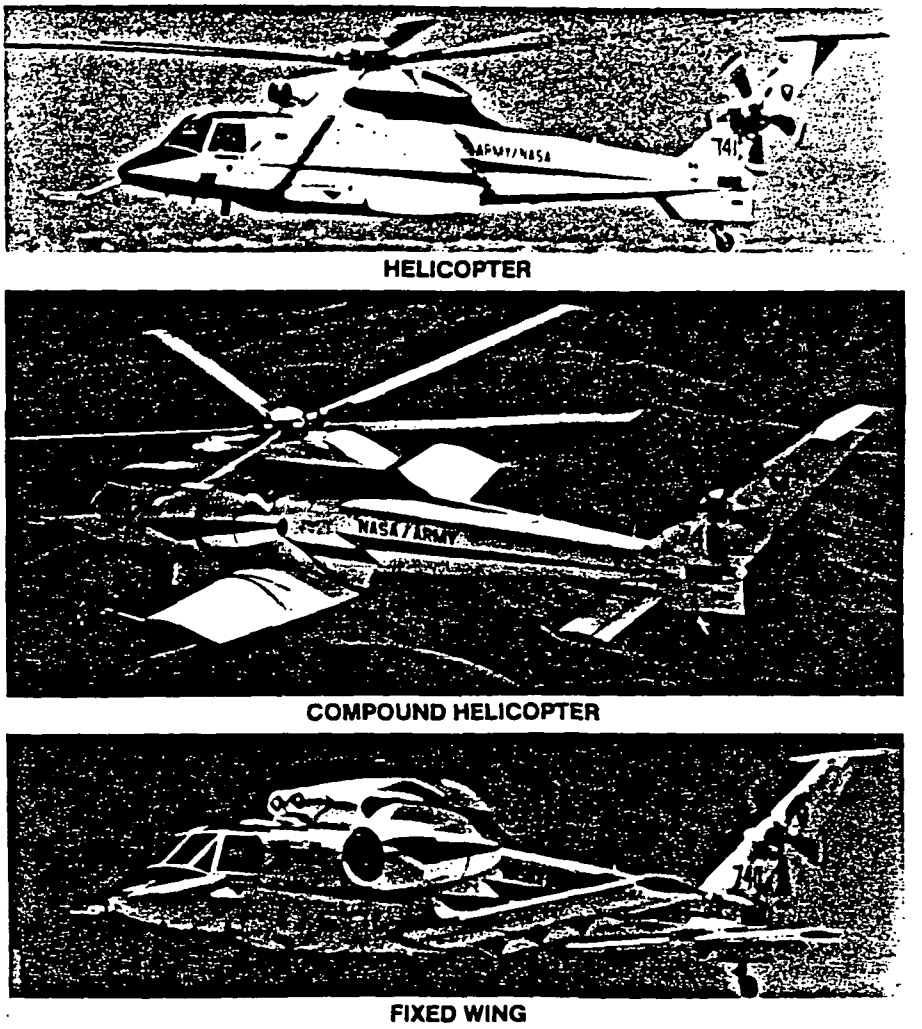

Figure 1

View of RSRA in Three Basic Configurations

NASA Ames-Dryden Flight Research Facility, Edwards Air Force Base, California. One of the goals of the fixed wing flight tests was to obtain time histories of the motion of the RSRA resulting from various control inputs, so that decoupled linear models of the RSRA's rigid body motion could be derived. These linear models were obtained using current system identification techniques which will be discussed in following chapters.

As with any flight test program, a computer simulation of anticipated flight conditions is essential prior to actual flight testing. The simulation can make accurate predictions of the dynamic behavior of the aircraft in flight and thus serve as a valuable pre-flight tool. The simulation can be used for pilot training and for designing aircraft control inputs for model identification purposes. The simulation can also be used in conjunction with flight test data to establish or refine new and existing control laws for implementation in both aircraft simulation and onboard autopilot systems.

The NASA RSRA simulation is based on the Sikorsky Aircraft General Helicopter (GENHEL) mathematical model, modified for the particular characteristics of the RSRA aircraft. The RSRA/GENHEL simulation employs a nonlinear mathematical model of the equations of motion combined with wind tunnel aerodynamic data to predict the motion of the aircraft.[1] It is capable of modeling the RSRA in any of its three possible configurations. The simulation is

operated by user-supplied inputs that indicate the desired flight conditions of the aircraft. Once these flight conditions have been selected, the operator may select a trim option and/or a predetermined dynamic maneuver. If a dynamic maneuver is selected, time histories of the resulting aircraft motion can be created. From these time histories, decoupled linear models of the rigid body motion can be obtained using methods that will be discussed in following chapters.

The reason for obtaining these linear models was twofold. First, the linear models derived from the simulation could be used as an inexpensive alternative to running the entire nonlinear simulation program. The nonlinear simulation cannot be run real time except on large computer systems, which becomes quite expensive and time consuming. The linear models can be run real time on nearly all computers, and very little time is required to do so. More importantly, as this report attempts to show, the linear models derived from the simulation can be used in many of the same applications as the nonlinear simulations with highly accurate results.

The second reason for obtaining linear models from both simulation and flight data was to perform a comparison between the two different models. Previously, there have been few comparisons between the RSRA simulation and flight data in any of the three possible aircraft configurations. Since the aircraft had never flown in the fixed wing mode,

the series of fixed wing flight tests presented an interesting and unique opportunity to investigate the correlation between the simulation-predicted data and the actual flight data. The linear models derived from both simulation and flight data were compared to examine the validity of the RSRA simulation as a tool for predicting aircraft behavior. Since the RSRA will be used as the base vehicle for other experimental aircraft, most notably the X-wing project, knowing the differences between RSRA simulation and flight test data in the fixed wing configuration will be highly beneficial to future research efforts with this aircraft.

CHAPTER 2

Theory

To describe the motion of a rigid aircraft in space with control surfaces fixed (i.e., control surfaces respond only to commanded inputs), a system is defined that consists of six degrees of freedom. These six degrees of freedom consist of three translational motions of the aircraft center of gravity (CG) and three rotational motions about the CG. These motions are generally represented in the aircraft body axes system as shown in Figure 2. The body axes system is an orthogonal right hand set, with origin of coordinates at the aircraft CG.

In order for the aircraft to be in equilibrium, the sum of all the forces or moments in each coordinate axis must be zero. Therefore, a total of six equilibrium equations is required. These six equations consist of gravitational, kinematic (including both translational and angular inertial forces), aerodynamic and propulsive components. The sum of all these effects results in the aircraft rigid body equations of motion given below.[2]

$$-mg \sin \theta - m(\dot{u} + wq - vr) + X + Fx = 0$$

$$mg \cos \theta \sin \phi - m(\dot{v} + ur - wp) + Y + Fy = 0$$

$$mg \cos \theta \cos \phi - m(\dot{w} + vp - uq) + Z + Fz = 0$$

$$-[\dot{p}Ixx - (Iyy - Izz)qr - Izx(\dot{r} + pq)] + L + Tx = 0$$

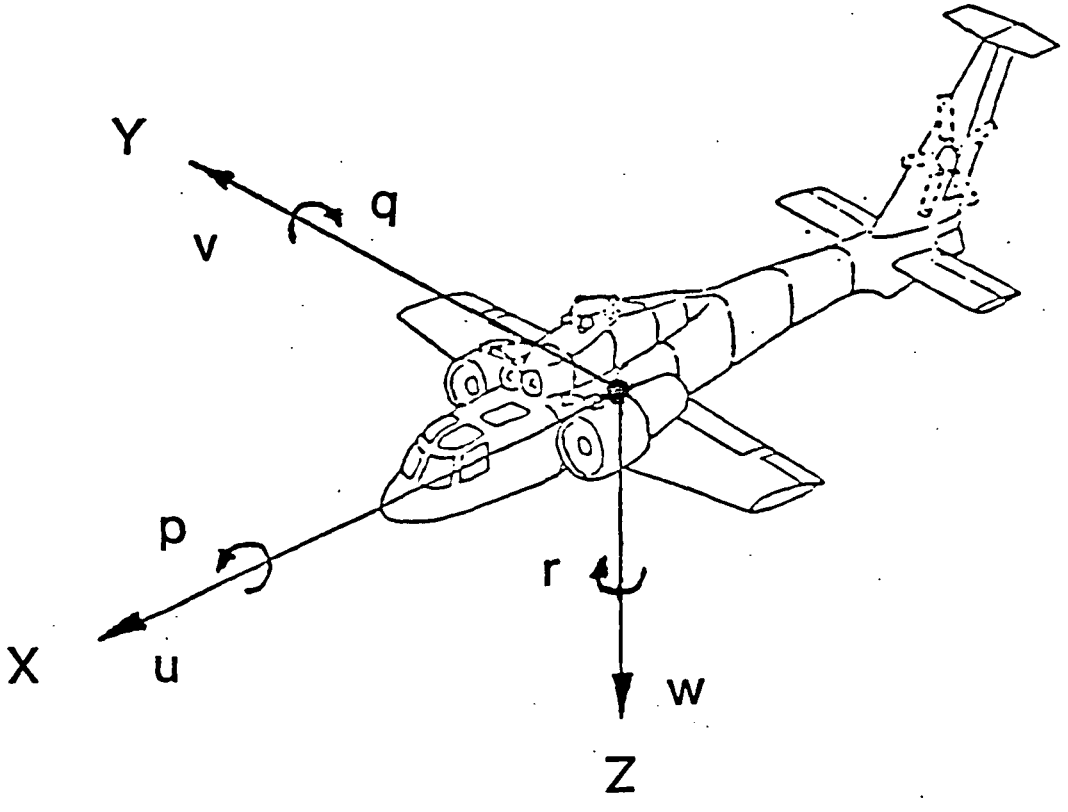

Figure 2

RSRA Fixed Wing Body Axes
Coordinate System

$$-[\dot{q}Iyy - (Izz - Ixx)pr - Izx(r^2 - p^2)] + M + Ty = 0$$

$$-[\dot{r}Izz - (Ixx - Iyy)pq - Izx(\dot{p} - qr)] + N + Tz = 0$$

where:

m = mass of the aircraft

g = local acceleration of gravity

[u,v,w] = body axes velocity components of CG

[p,q,r] = body axes angular velocity components about CG

[X,Y,Z] = aerodynamic forces acting on CG

[L,M,N] = aerodynamic moments acting about CG

[θ,ϕ] = aircraft attitude and bank angles respectively

[Fx,Fy,Fz] = propulsive forces acting on CG

[Tx,Ty,Tz] = propulsive moments acting about CG

To eliminate the orientation (Euler) angles θ and ϕ from the equations of motion, the following equations relating the orientation angles and angular rates to the body axes angular velocities are also required.

$$\dot{\theta} = q \cos \phi - r \sin \phi$$

$$\dot{\phi} = p + \tan \theta \, (r \cos \phi + q \sin \phi)$$

These equations represent a system of eight fully coupled nonlinear differential equations and as such must be solved simultaneously. Since in general the aerodynamic forces and moments are functions of the translational and angular velocities and control inputs, these equations have aerodynamic coupling as well as inertial and gravitational coupling. Due to the complexity of solving this large

system of equations, methods are sought which simplify their solution while retaining accuracy. This is the goal of linear modeling.

Utilizing the theory of small perturbations, the non-linear equations of motion are represented by linear equations. This is accomplished by expanding each of the terms in the equations of motion by Taylor series expansion, and neglecting second order and higher terms. If the disturbances from the aircraft's equilibrium state are small, a good approximation of the motion of the aircraft can be obtained. If, in addition, the aircraft is symmetric and is in symmetric equilibrium flight, then the linearized equations of motion decouple into two sets of four equations known as the control surface fixed longitudinal and lateral sets of equations.[2]

Longitudinal Set

$$(-mg \cos \theta) \theta - m(\dot{u} + Wq) + X_u u + X_w w + X_q q = \text{input}$$

$$(-mg \sin \theta) \theta - m(\dot{w} + Uq) + Z_u u + Z_w w + Z_q q = \text{input}$$

$$-(\dot{q} Iyy) + M_u u + M_w w + M_q q = \text{input}$$

$$\dot{\theta} = q$$

Lateral Set

$$(mg \cos \theta)\, \phi - m(\dot{v} - Wp + Ur) + Y_v v + Y_p p + Y_r r = \text{input}$$

$$-(\dot{p} Ixx - \dot{r} Izx) + L_v v + L_p p + L_r r = \text{input}$$

$$-(\dot{r} Izz - \dot{p} Izx) + N_v v + N_p p + N_r r = \text{input}$$

$$\dot{\phi} = p$$

where:

[U,V,W] = body axes velocities at trim condition

[P,Q,R] = body axes angular velocities at trim condition

[Θ_1 , Φ] = pitch and roll attitude at trim condition

As seen above, the longitudinal set of equations involves the state variables u,w,q and θ only, and the lateral set of equations involves the state variables v,p,r and ϕ only. These two sets of decoupled equations represent a substantial reduction in the computational labor required to solve the rigid body equations of motion. Furthermore, these decoupled equations of motion should produce very accurate results if the assumptions used in their derivation are valid for the aircraft in question.

The typical solution to the longitudinal set of equations results in two oscillatory modes of motion known as the short period mode and the phugoid mode. The short period mode is a high frequency, heavily damped motion. The motion is composed primarily of the vertical velocity (w) and the pitch rate (q). Because this mode generally decays very rapidly, the short period motion is seldom noticeable to pilots. In contrast, the phugoid mode is a lightly damped, low frequency motion that is composed primarily of the forward velocity (u) and the pitch attitude (θ). Although the phugoid is generally lightly damped, the period of the motion is large enough so that the aircraft is easily controlled.

The typical solution to the lateral set of equations results in one oscillatory mode and two simple modes. The oscillatory mode is known as the Dutch Roll mode. The numerically larger simple root is called the roll subsidence mode, and the numerically smaller simple root is known as the spiral mode. The Dutch Roll mode is a high frequency motion that is fairly heavily damped, much like the longitudinal short period motion. The Dutch Roll mode involves a combination of rolling and yawing motions, primarily consisting of the roll rate (p), and the yaw rate (r). Despite what its name may imply, the Dutch Roll mode is generally more excited by rudder input than by aileron input. The roll subsidence mode is a very heavily damped simple motion that is almost completely due to the roll damping of the wings. Because of this, the roll subsidence mode is composed primarily of the roll rate (p). Since this mode decays so rapidly, it is rarely noticeable to pilots. The spiral mode is a simple motion that is usually lightly damped or possibly divergent. This motion primarily consists of the roll angle (ϕ). If this mode is divergent, the aircraft will go into a spiral dive if not controlled. However, even if the root is positive (unstable), the time to double amplitude is generally large enough that the motion will diverge slowly, and thus can be easily controlled by the pilot.

The longitudinal and lateral sets of equations represent the system that has been chosen to model the

aircraft's rigid body motion. Since this system representation was known a priori to be very accurate in describing aircraft motion, it was not necessary to develop a new system representation. The process of developing an overall model from input/output information that represents a particular dynamic system is called system identification. The system identification process consists of three basic steps:

1. Model structure determination,
2. Parameter identification, and
3. Model validation.

Since in this case a model structure was already known, only the parameter identification and model validation steps were required. Parameter identification is the process of determining the value of each individual member of a predetermined system model. Model validation establishes the fidelity with which the chosen system representation models the actual system dynamics.

For the purposes of determining aircraft rigid body dynamics, parameter identification is used to extract numerical values for the aerodynamic stability derivatives and control coefficients from time histories of the aircraft dynamics. These time histories are generated about a specified trim condition and may be obtained from flight test data or created by computer simulation.

The linearized longitudinal and lateral sets of equations can be represented in state space form[3] as follows:

$$\dot{x}(t) = Fx(t) + Gu(t)$$

where:

$x(t)$ = vector of longitudinal or lateral state variables

$u(t)$ = vector of control surface inputs

F = matrix containing identified force and moment coefficients

G = matrix containing identified control coefficients

Here it is recognized that the F and G matrices are normalized in the conventional manner such that the force coefficients are divided by mass and the moment coefficients are divided by the relevant moment of inertia.

Once the longitudinal and lateral F and G matrices have been identified for specified initial conditions, the rigid body response to any control input can be simulated by solving the state space equation (linear model) shown above.

CHAPTER 3

Procedure

Simulation Identification Methodology

The overall identification methodology for the linear models derived from the nonlinear simulation is shown in Figure 3. The first step was to identify dynamic control inputs that would sufficiently excite the rigid body modes of the aircraft. These input profiles, along with predetermined aircraft trim conditions, were then put into the GENHEL nonlinear simulation, where time histories of the resulting aircraft motion were generated. The regression input data were established by separating the longitudinal and lateral state variable and control surface time histories. These time histories were then input to the Optimal Subset Regression program which identified the aerodynamic force and moment coefficients. Finally, the known kinematic and gravitational components were added with a linear model composition routine to establish the decoupled linear models. A detailed discussion of this procedure follows.

To obtain a good linear model identification, it is necessary to excite the natural modes of motion of the aircraft. Therefore, the correct choice of dynamic inputs becomes vital to producing accurate results. If the given inputs do not contain the proper frequencies certain

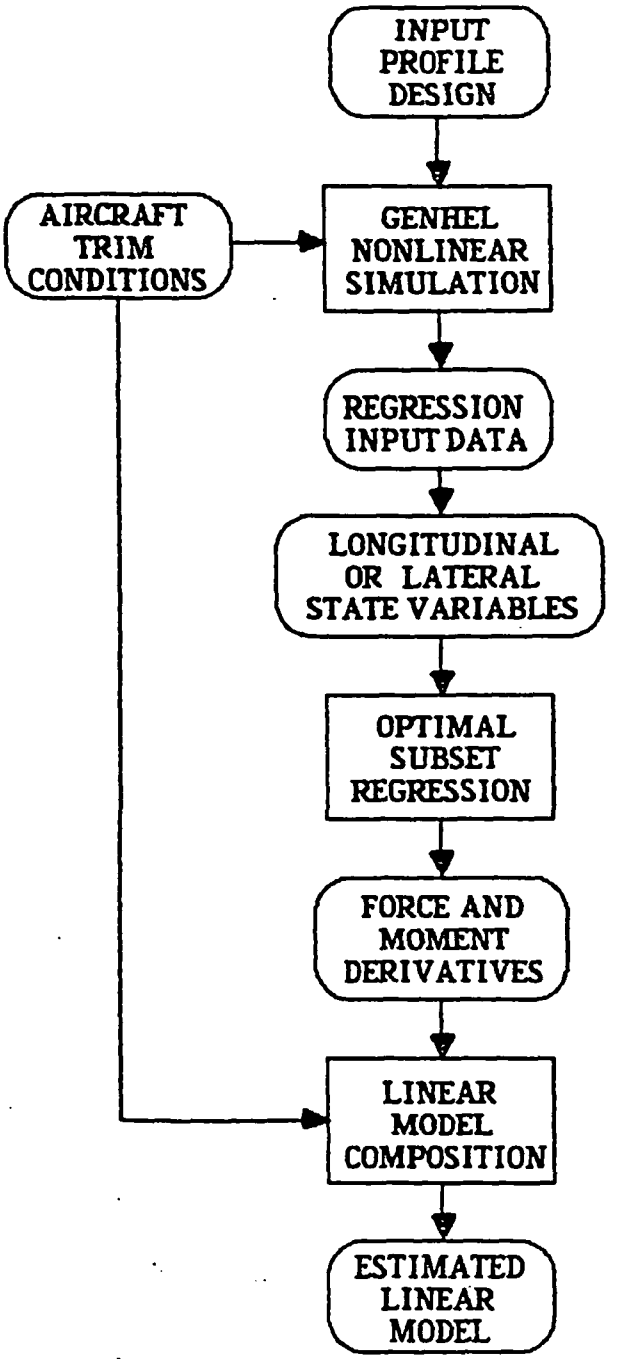

Figure 3

Simulation Linear Model Identification Methodology

aircraft modes may not be excited, resulting in poor model identification. Likewise, if the inputs do not contain sufficient energy (i.e., control surface deflection), then only partial excitation of the aircraft modes may occur, again resulting in a poor identification. Since the frequencies of the aircraft modes were not fully known, it was crucial that the first dynamic inputs to the simulation covered a range of frequencies so that both low and high frequency aircraft modes were activated. Therefore, the initial input chosen for both the longitudinal and lateral mode identification was a 3211 input. This input consists of alternating steps which are held for relative durations of 3, 2, 1 and 1 time units. The 3211 input has a relatively broad frequency bandwidth and for this reason was thought to be a better choice for the initial model identification than either a doublet or a discrete frequency sine wave input. To ensure an unbiased model identification, baseline aircraft trim conditions were established using the GENHEL simulation trim option. A summary of important aircraft characteristics from trim conditions is shown in Appendix A. In order to investigate the effects of airspeed, trim conditions were found for two different airspeeds: 160 KCAS and 200 KCAS.

For the longitudinal models the 3211 inputs consisted of horizontal tail deflections. (On the RSRA the horizontal tail and the elevator are rigidly geared and move together as a unit.) These inputs were applied at both

airspeeds. For the lateral models the 3211 inputs consisted of aileron deflections performed at both airspeeds and, in addition, a 3211 rudder input was used at 200 KCAS. The rudder input was used to better identify the directional stability derivatives of the lateral case. Since the identification process for the different airspeeds was identical, only the 200 KCAS case will be explained in further detail.

With the 3211 input profile selected, the RSRA GENHEL nonlinear simulation was used to obtain time histories of the resulting aircraft motion. A typical control input time history displaying a 3211 pedal (rudder) input is presented in Figure 4. As seen in Figure 4, the initial

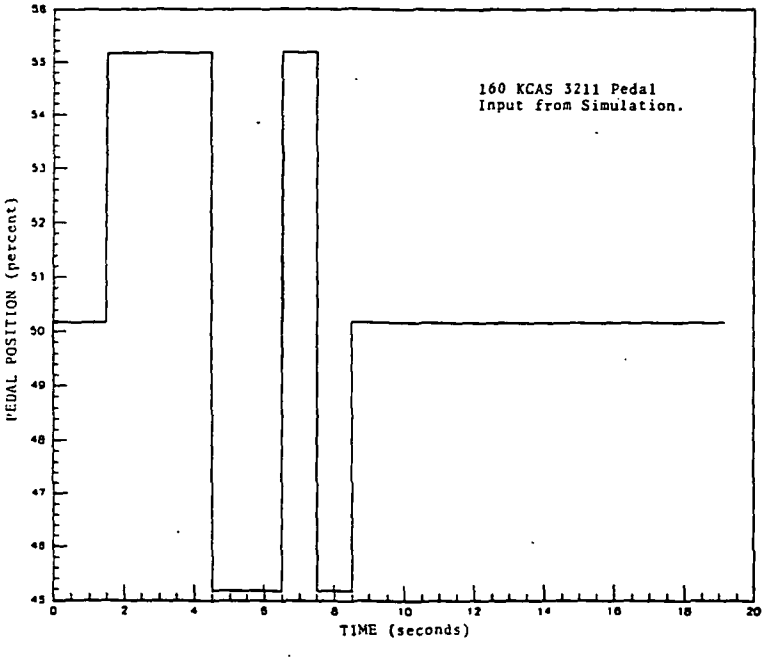

Figure 4

Typical 3211 Input Profile

pedal position, in percent, represents the baseline aircraft trim value. The horizontal tail and aileron 3211 inputs were deflected $\pm$7% of stick authority from the trim position. The rudder input was held to $\pm$5% of the trim pedal position. These inputs generated disturbances of less than 15° in pitch attitude and about 40° in roll attitude. Thus, for the purposes of the flight test program, these dynamic inputs could be duplicated with reasonable accuracy while remaining in the safe aircraft operating envelope.

Since the linearized equations of motion were assumed to decouple into two distinct sets, the presence of any significant coupling would invalidate the chosen linear model structure. For this reason, the nonlinear simulation time histories resulting from the 3211 inputs were examined to determine whether any significant coupling was present.

Figures 5 and 6 show the nonlinear simulation response of the body axes velocities to the horizontal tail 3211 input. The responses of u, v and w presented in Figure 5 clearly show the decoupled nature of the aircraft motion. The maximum (peak to peak) disturbance of u was more than 20 times that of v, and the maximum disturbance of w was more than 150 times that of v. This comparison illustrates the anticipated longitudinal and lateral decoupling, and also shows that the horizontal tail input excited w much more effectively than u. In Figure 6, the responses of p, q and r are shown. Virtually complete decoupling between

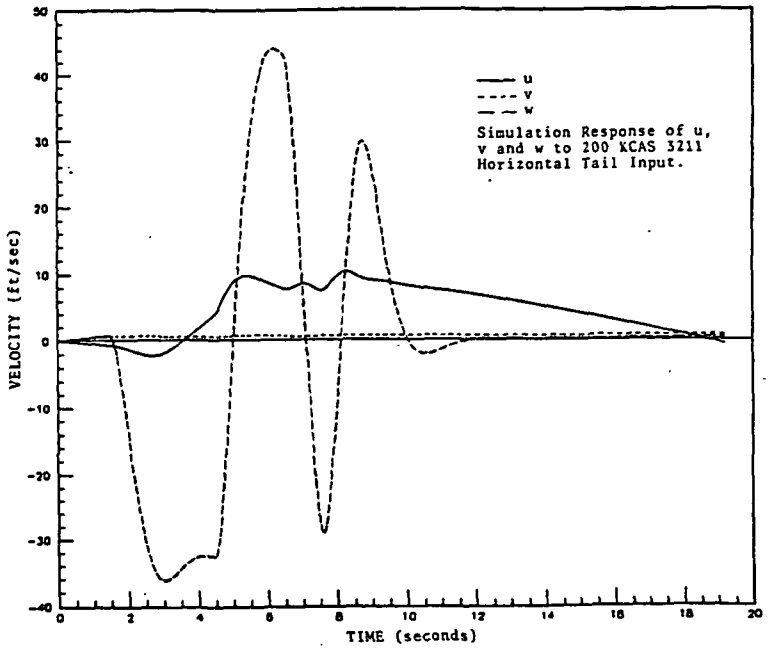

Figure 5

Response of Body Axes Velocities to 3211 Horizontal Tail Input

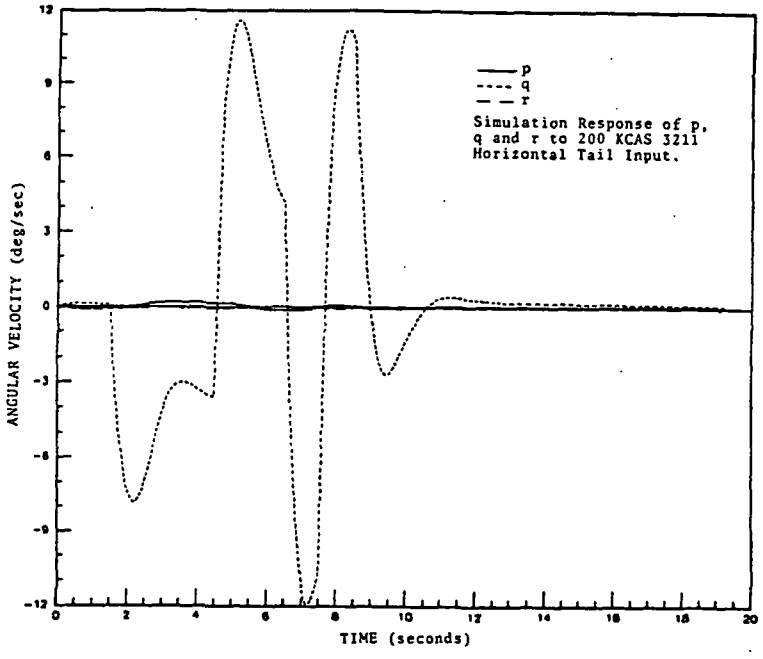

Figure 6

Response of Body Axes Angular Rates to 3211 Horizontal Tail Input

the longitudinal and lateral angular rates is seen in this comparison.

Figure 7 presents the responses of u, v and w to the rudder 3211 input. It is seen in this comparison that while u and w were mildly excited, the maximum disturbance of v was more than eight times that of u or w. In Figure 8, the responses of the angular rates p, q and r to the aileron 3211 input are presented. This comparison shows that only p was well excited, about nine times more than r and 25 times more than q. Again, not only were the longitudinal and lateral motions seen to be decoupled, but the off-axis motion r was only mildly excited compared with the roll rate p, produced by the aileron input. This is analogous to the effect the horizontal tail input had on the responses of u and w as seen in Figure 5.

From the foregoing comparisons, it is clear that very little coupling exists between longitudinal and lateral motions, thus the decoupled model structure is valid and should produce excellent results.

With the validity of the decoupled linear model structure established, the nonlinear simulation time histories of the longitudinal and lateral state variables were separated into three groups. These included one longitudinal group of time histories corresponding to the horizontal tail input, and two lateral groups, one corresponding to the aileron input and one to the rudder input. Each of these groups of time histories were then input to the Optimal

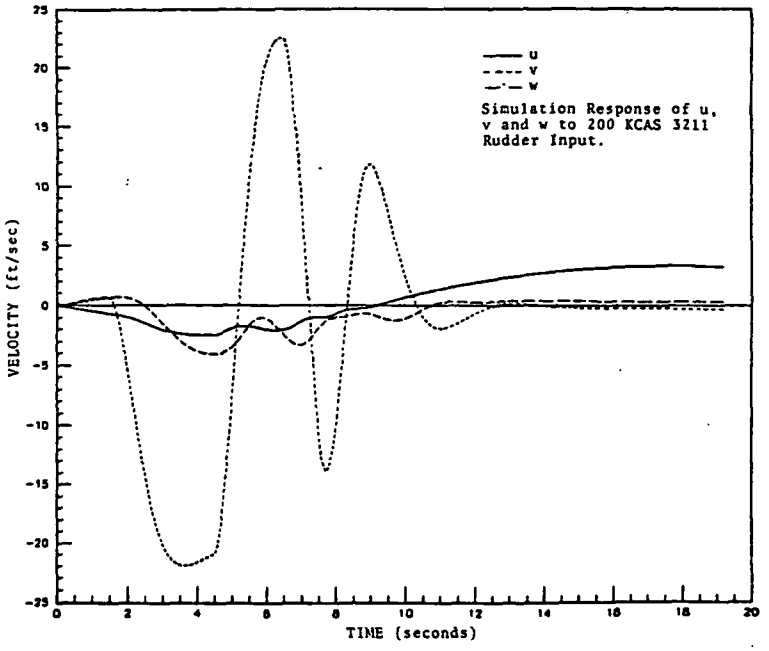

Figure 7

Response of Body Axes Velocities to 3211 Rudder Input

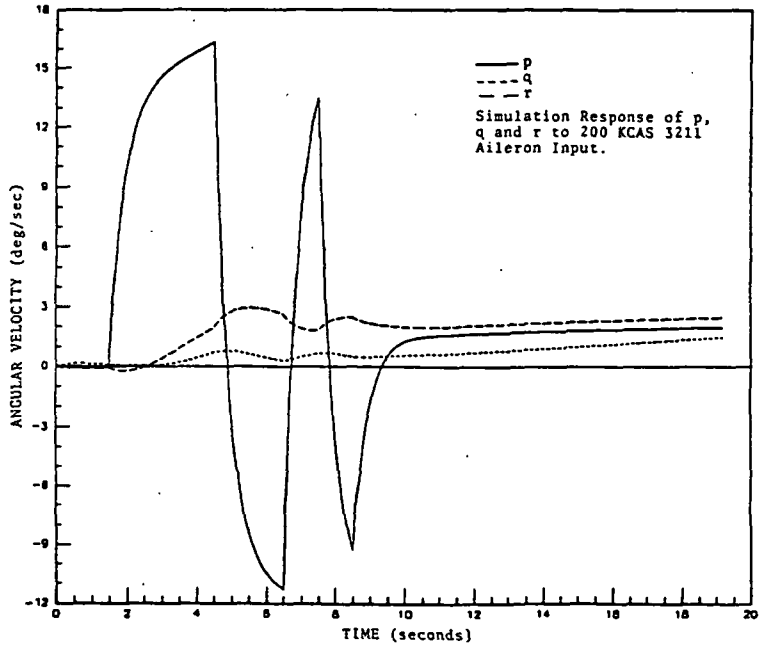

Figure 8

Response of Body Axes Angular Rates to 3211 Aileron Input

Subset Regression (OSR) program.[4] The OSR program correlates the time histories of the aircraft state variables and control inputs (independent variables) to the aerodynamic force and moment coefficients (dependent variables).

The program uses a stepwise regression technique to determine the independent variables included in the model. Therefore, the number of independent variables used to describe a given dependent variable is not predetermined as in a standard least squares approximation. The OSR program chooses the independent variables based on whether they are available for inclusion relative to the predetermined linear model structure, and based on their correlation with the given dependent variable. The program will choose sequentially the independent variables from the highest correlated to the lowest, while simultaneously evaluating the F-ratio of each independent variable before it is entered. The general Fisher F-ratio for a candidate model is given by:[5]

$$F = \frac{(R^2/m)}{(1-R^2)/(N-m)}$$

where:

R^2 = Multiple Correlation Coefficient

N = Number of data points

m = Number of independent variables

The F-ratio is seen to be a function of the number of variables describing the dependent variable as well as the multiple correlation coefficient. The F-ratio, therefore, is used to determine whether the addition of a given independent variable is justified, since the model grows more complicated as it grows larger. The F-ratio can also simplify the model by dismissing independent variables already present, if the increased accuracy is slight compared with the complication of solving the larger system. This ensures that the optimal model in terms of both accuracy and ease of solution will be selected. For the linear model identification, the OSR program used a sampling rate of 83.3 Hz over a time history containing 1600 data points, or approximately 19 seconds of real time data. Since the fastest of the rigid body modes was not expected to exceed 1.0 Hz, the sampling rate was more than adequate to prevent modeling inaccuracies due to insufficient data sampling. The OSR program output consisted of one longitudinal model and two lateral models of aerodynamic force and moment coefficients and control coefficients.

Since the OSR program extracted only the aerodynamic force and moment coefficients, the linearized gravitational and kinematic force components obtained from aircraft trim conditions were then added to each of the linear models. This produced the first complete set of F and G matrices, or linear models: one longitudinal model produced by the horizontal tail input, and two lateral models, one each

produced by the aileron and rudder inputs. The F matrices of each model were then analyzed to determine the characteristic roots or eigenvalues of each identified system. The eigenvalues define the natural rigid body modes of the aircraft. Finally, the eigenvectors or mode shapes which describe in a relative sense which independent (state) variables are more prevalent in the composition of a particular rigid body mode were determined.

The results for the 200 KCAS model identification are presented in Tables 1 to 3. The longitudinal linear model, along with its eigenvalues and eigenvectors, is shown in Table 1. The aileron-produced lateral model, along with its eigenvalues and eigenvectors, is shown in Table 2, and the rudder-produced results are shown in Table 3.

With one complete set of models established for both the longitudinal and lateral cases, the entire identification procedure was repeated. This time a discrete frequency sine wave input profile was specified. For the longitudinal model identification, the amplitude of the sine wave input to the horizontal tail was held at $\pm$7% stick authority. The frequency of the sine wave input used was the short period natural frequency obtained with the 3211 input. This input was used to further excite the short period mode which in turn would cause a more accurate identification of the longitudinal linear model.

Likewise, for the lateral model, the amplitude of the rudder input was held at $\pm$5% pedal authority, and the

Table 1

Preliminary 200 KCAS Longitudinal
Results from 3211 Input

$$F = \begin{bmatrix} -.025 & .016 & 1.37 & -32.2 \\ .188 & -.828 & 385. & .565 \\ .0009 & -.0101 & -2.04 & 0 \\ 0 & 0 & 0 & 1 \end{bmatrix} \quad x = \begin{bmatrix} u \\ w \\ q \\ \theta \end{bmatrix}$$

$$G = \begin{bmatrix} .211 \\ -2.16 \\ -.440 \\ 0 \end{bmatrix} \quad u = \begin{bmatrix} \delta_{HT} \end{bmatrix}$$

	Short Period Mode	Phugoid Mode
Eigenvalues:	$-1.44 \pm 1.87i$	$-.0114 \pm .124i$
Eigenvectors:	$\begin{bmatrix} .0236 \pm .0099i \\ 1.000 \\ -.0016 \pm .0049i \\ .0020 \pm .0007i \end{bmatrix}$	$\begin{bmatrix} 1.000 \\ -.0048 \pm .0047i \\ .0005 \\ -.0004 \pm .0038i \end{bmatrix}$

Table 2

Preliminary 200 KCAS Lateral Results
from 3211 Aileron Input

$$F = \begin{bmatrix} -.164 & 32.2 & -1.14 & -404. \\ 0. & 0. & 1. & 0. \\ .0178 & 0. & -2.26 & -1.12 \\ .0053 & 0. & .101 & -.917 \end{bmatrix} \quad x = \begin{bmatrix} v \\ \phi \\ p \\ r \end{bmatrix}$$

$$G = \begin{bmatrix} -.0051 \\ 0. \\ .396 \\ -.0136 \end{bmatrix} \quad u = \begin{bmatrix} \delta_{AIL} \end{bmatrix}$$

	Dutch Roll Mode	Roll Subsidence Mode	Spiral Mode
Eigenvalues:	$-.568 \pm 1.47i$	-2.27	$.0593$
Eigenvectors:	$\begin{bmatrix} 1.000 \\ -.0037 \pm .0033i \\ .0070 \pm .0035i \\ .0007 \pm .0039i \end{bmatrix}$	$\begin{bmatrix} 1.000 \\ .110 \\ -.249 \\ .0147 \end{bmatrix}$	$\begin{bmatrix} 1.000 \\ .0811 \\ .0048 \\ .0059 \end{bmatrix}$

Table 3

Preliminary 200 KCAS Lateral Results
from 3211 Rudder Input

$$F = \begin{bmatrix} -.249 & 32.2 & 0. & -388. \\ 0. & 0. & 1. & 0. \\ .0021 & 0. & -2.20 & 1.48 \\ .008 & 0. & -.068 & -.184 \end{bmatrix} \quad x = \begin{bmatrix} v \\ \phi \\ p \\ r \end{bmatrix}$$

$$G = \begin{bmatrix} -.169 \\ 0. \\ -.0215 \\ .0556 \end{bmatrix} \quad u = \begin{bmatrix} \delta_{RUD} \end{bmatrix}$$

	Dutch Roll Mode	Roll Subsidence Mode	Spiral Mode
Eigenvalues:	$-1.09 \pm 1.62i$	-2.17	.0612
Eigenvectors:	$\begin{bmatrix} 1.000 \\ -.0014 \pm .0015i \\ -.0010 \pm .0039i \\ .0020 \pm .0040i \end{bmatrix}$	$\begin{bmatrix} 1.000 \\ -.0553 \\ .1203 \\ .0004 \end{bmatrix}$	$\begin{bmatrix} 1.000 \\ .0590 \\ .0036 \\ .0041 \end{bmatrix}$

amplitude of the aileron input was held at ±7% stick authority. Since the rudder generally causes greater excitation of the Dutch Roll mode than the aileron, the frequency used for both sine wave control inputs was the Dutch Roll frequency obtained from the 3211 rudder input. Using these sine wave input profiles, time histories were again generated by the GENHEL nonlinear simulation and the model identification process repeated.

The results for the model identification utilizing the sine wave inputs are shown in Tables 4 through 6. The longitudinal linear model, along with its associated eigenvalues and eigenvectors, is shown in Table 4. Similar results for the aileron-produced lateral model are presented in Table 5, and the results for the rudder-produced model are given in Table 6.

Flight Data Identification Methodology

The overall methodology for the flight data linear model identification is shown in Figure 9. The RSRA fixed wing flight tests were conducted at the NASA Ames-Dryden Flight Research Facility during the summer of 1984. The input profiles selected for the flight test program included 2311, doublet and sine sweep maneuvers. Required aircraft state variables which were not recorded during flight testing were estimated with an extended Kalman filter and fixed interval smoother. This created the necessary regression input data for the linear model identification. Since the remaining flight data identification

Table 4

Preliminary 200 KCAS Longitudinal
Results from Sine Wave Input

$$F = \begin{bmatrix} -.0066 & .0211 & .940 & -32.2 \\ -.169 & -.808 & 390. & .565 \\ .0012 & -.0092 & -2.00 & 0 \\ 0 & 0 & 1 & 0 \end{bmatrix} \quad x = \begin{bmatrix} u \\ w \\ q \\ \theta \end{bmatrix}$$

$$G = \begin{bmatrix} .179 \\ -1.40 \\ -.423 \\ 0 \end{bmatrix} \quad u = \begin{bmatrix} \delta_{HT} \end{bmatrix}$$

	Short Period Mode	Phugoid Mode
Eigenvalues:	$-1.41 \pm 1.79i$	$-.0028 \pm .125i$
Eigenvectors:	$\begin{bmatrix} .0217 \pm .0081i \\ 1.000 \\ -.0015 \pm .0046i \\ .0020 \pm .0007i \end{bmatrix}$	$\begin{bmatrix} 1.000 \\ .0241 \pm .0066i \\ .0005 \\ -.0001 \pm .0039i \end{bmatrix}$

Table 5

Preliminary 200 KCAS Lateral Results
from Aileron Sine Wave Input

$$F \approx \begin{bmatrix} -.249 & 32.2 & -.605 & -388. \\ 0. & 0. & 1. & 0. \\ .0105 & 0. & -2.26 & .647 \\ .0066 & 0. & .0855 & -1.23 \end{bmatrix} \qquad x = \begin{bmatrix} v \\ \phi \\ p \\ r \end{bmatrix}$$

$$G \approx \begin{bmatrix} 0. \\ 0. \\ .405 \\ -.0144 \end{bmatrix} \qquad u = \begin{bmatrix} \delta_{AIL} \end{bmatrix}$$

	Dutch Roll Mode	Roll Subsidence Mode	Spiral Mode
Eigenvalues:			
	$-.740 \pm 1.57i$	-2.34	.0785
Eigenvectors:	$\begin{bmatrix} 1.000 \\ -.0030 \pm .0003i \\ .0027 \pm .0045i \\ .0010 \pm .0041i \end{bmatrix}$	$\begin{bmatrix} 1.000 \\ .121 \\ -.284 \\ .0159 \end{bmatrix}$	$\begin{bmatrix} 1.000 \\ .0762 \\ .0060 \\ .0055 \end{bmatrix}$

Table 6

Preliminary 200 KCAS Lateral Results
from Rudder Sine Wave Input

$$F = \begin{bmatrix} -.248 & 32.2 & 0. & -388. \\ 0. & 0. & 1. & 0. \\ .0019 & 0. & -2.68 & 2.09 \\ .0079 & 0. & .197 & -1.97 \end{bmatrix} \qquad x = \begin{bmatrix} v \\ \phi \\ p \\ r \end{bmatrix}$$

$$G = \begin{bmatrix} -.170 \\ 0. \\ -.0325 \\ .0563 \end{bmatrix} \qquad u = \begin{bmatrix} \delta_{RUD} \end{bmatrix}$$

	Dutch Roll Mode	Roll Subsidence Mode	Spiral Mode
Eigenvalues:	$-1.02 \pm 1.55i$	-2.93	$.0645$
Eigenvectors:	$\begin{bmatrix} 1.000 \\ -.0018 \pm .0015i \\ -.0006 \pm .0043i \\ .0018 \pm .0039i \end{bmatrix}$	$\begin{bmatrix} 1.000 \\ .0292 \\ -.0854 \\ .0093 \end{bmatrix}$	$\begin{bmatrix} 1.000 \\ .0610 \\ .0039 \\ .0043 \end{bmatrix}$

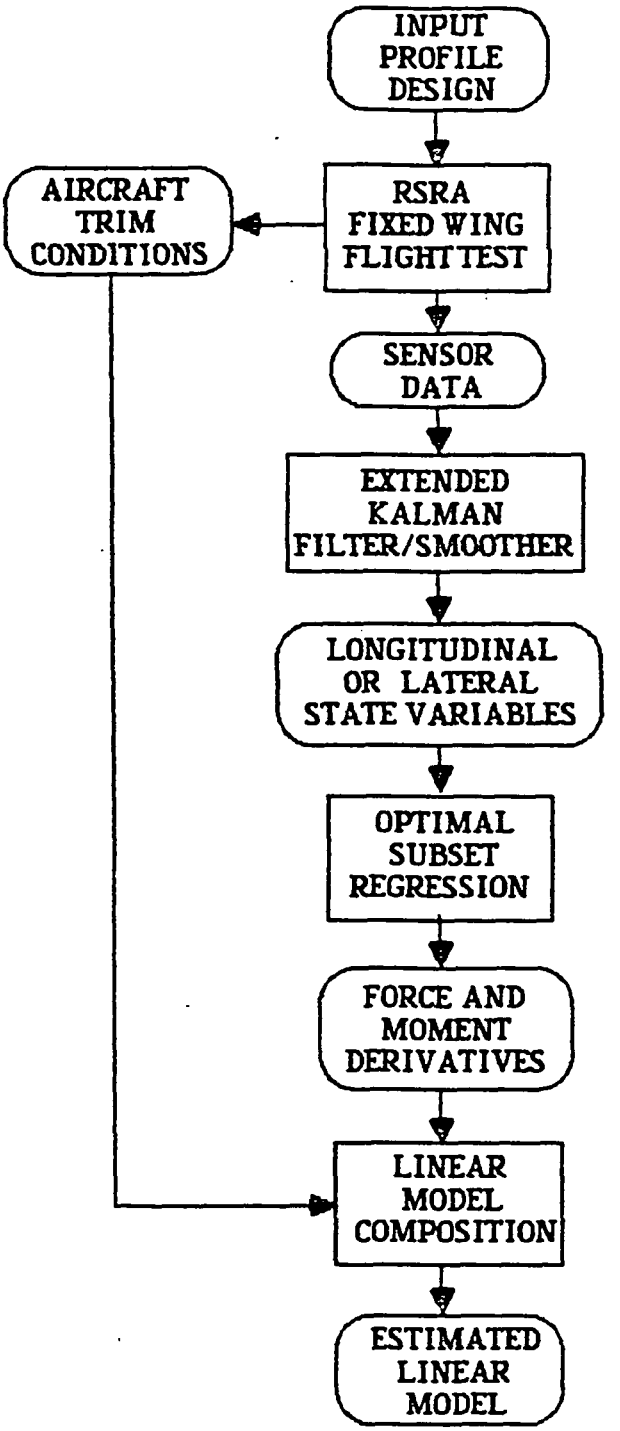

Figure 9

Flight Data Linear Model Identification Methodology

methodology is the same as that of the simulation methodology detailed previously, it will not be discussed further.

The first flight of the RSRA in the fixed wing configuration was completed in May 1984. The flight test plan included performance, acoustic and parameter identification experiments, and was conducted over the period of May through September 1984.

For the parameter identification tests, a number of input profiles were used. These included 2311 and doublet inputs, and also sine sweep maneuvers. The 2311 input is similar to the 3211 input profile but reverses the duration of the first two stick motions. The sine sweep maneuver consisted of a series of increasing frequency sine wave input profiles. These inputs were designed to excite the band of frequencies between roughly .05 Hz and 1.0 Hz, rather than provide a discrete frequency excitation. This is approximately the range of frequencies where the simulation-derived linear models predicted the rigid body modes to occur. Therefore this input profile, while unfeasible for use with the GENHEL computer simulation due to its long duration (up to 80 seconds), was ideal for flight testing purposes because of its ability to excite all rigid body modes with a single maneuver. A typical sine sweep maneuver displaying the motion of the right aileron is shown in Figure 10. This maneuver was performed exceptionally well, as were all the required flight control

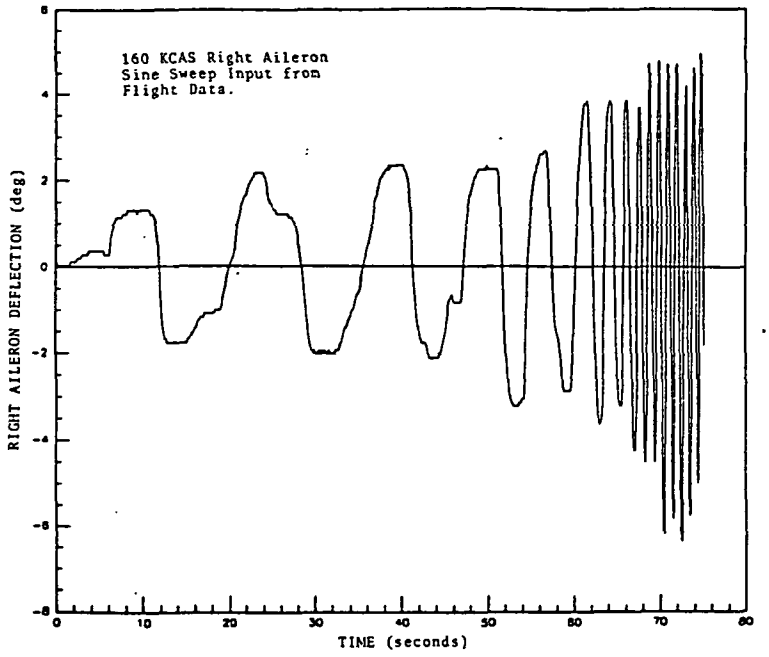

Figure 10

Right Aileron Sine Sweep Input

inputs. The test flights were piloted by Warren Hall of NASA Ames and Lt. Col. Pat Morris of the U.S. Army Aeromechanics Laboratory. All maneuvers used for identification purposes were performed with the aircraft Stability Augmentation System off to ensure that only the natural characteristics would be identified. To ensure adequate yaw control at low speed (below rotation speed), the tail rotor was left installed on the aircraft but was not used for yaw control once the aircraft was safely airborne. Also, to eliminate lower horizontal tail shake, the wing incidence was adjusted to 5° with 5° flap added. A summary of important aircraft trim conditions from the flight test data is shown in Appendix B.

To again verify that the actual aircraft dynamics were decoupled, a comparison of the responses of p and q was performed. This comparison, shown in Figure 11, gives the responses of p and q to an aileron sweep input. This comparison shows that at very low frequencies the motion, while mildly excited, is well decoupled, displaying only a trace of q excitation. At higher frequencies where p is highly excited, the small pitch rate that is apparent is caused by longitudinal (horizontal tail) inputs which become unavoidable at the high frequency of the aileron input. From this comparison it is apparent that no significant coupling occurs in the actual flight dynamics, and thus the decoupling assumption is again valid.

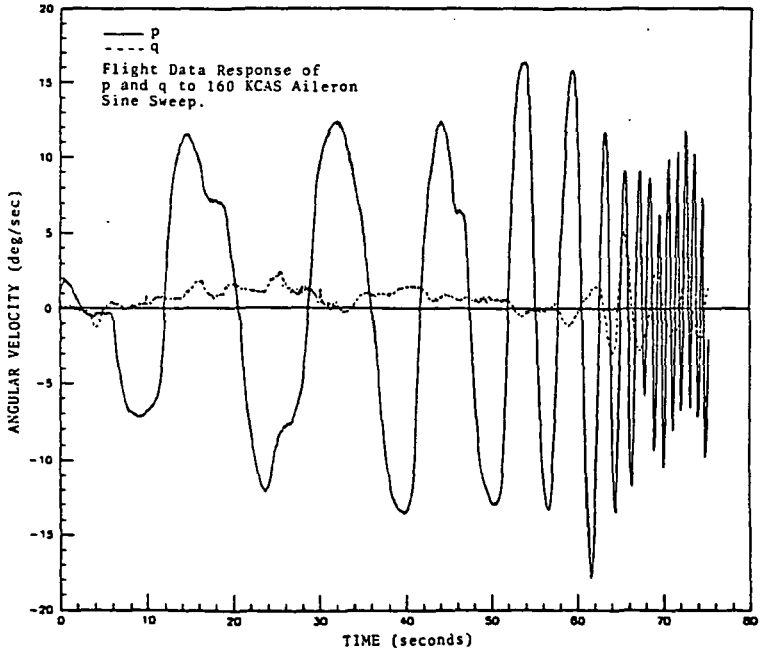

Figure 11

Response of Pitch and Roll Rates
to Aileron Sine Sweep

The identification of the linear models from the flight data followed nearly the same procedure as the simulation identification process. The primary difference was the necessity to estimate certain parameters that were missing from the flight data time histories. These aircraft state variables could not be measured directly due to lack of proper aircraft instrumentation.

The aircraft states that could not be directly measured during flight testing included the three body axes velocity components u, v and w. The aircraft states that were directly measured included θ and ϕ, all angular velocities and accelerations, and the translational accelerations, a_x, a_y, and a_z. By combining these measured data with the aircraft equations of motion, estimations u, v and w could be obtained. This process was accomplished with the Discrete Extended Kalman Filter and Fixed Interval Smoother (DEKFIS) program. A detailed discussion of the DEKFIS program is beyond the scope of this report, so only a general discussion of its use follows. The reader is referred to Mohr's guide[6] for a complete discussion of the DEKFIS program and its capabilities.

Consider the ith time step of a system with N data points, such that:

$$t_{i+i} = t_i + \Delta t$$

where:

$$t_o = 0$$

$$i = 0, 1, \ldots N$$

Further consider the system of the aircraft rigid body nonlinear equations of motion. The DEKFIS program will first linearize the equations of motion about t_i. It will then solve these linearized equations at t_{i+1}, and produce estimates of the desired parameters (u, v and w) based on statistical information from the measured aircraft data. With complete information now available at t_{i+1}, DEKFIS will again take the nonlinear equations of motion and linearize about the point t_{i+1}, and estimate u, v and w for the next time step, t_{i+2}, and so on. With this continuous process of linearizing about the most current estimation, the Extended Kalman Filter approach used in DEKFIS can provide very accurate estimates of missing states.

Once the time histories of the estimates of u, v and w had been obtained, the identification process was continued and flight data-derived linear models were generated. Due to the excessive labor involved in the flight data estimation process, flight data results were available at 160 KCAS only at the time of this report. It is anticipated that linear models identified from 200 KCAS flight data will be available in the near future.

Determination of Final Linear Models

The final longitudinal and lateral linear models were determined by combining the preliminary identification results with a practical engineering knowledge of fixed wing aircraft dynamics. An overview of this procedure for the case of the 200 KCAS simulation identification follows.

Similar procedures were used to determine the overall simulation and flight data models at 160 KCAS. The overview will focus on the selection of two important parameters: Xu and Lv.

The identification of force derivatives in the x-direction was complicated by the lack of appropriate control inputs. Since there was no control that provided direct excitation of fore-aft motion (i.e., thrust modulation), only partial excitation of the phugoid mode, through horizontal tail inputs, was possible. Because of this, the force derivatives in the x-direction displayed significantly lower R^2 and F-ratio values compared to the Z and M force and moment derivatives. The force and moment coefficients for the longitudinal identifications, along with the R^2 and F-ratio values, are shown in Table 7. As seen in Table 7, the absolute value of Xu (speed brake term) is greater for the 3211 input than the sine wave input. Because the 3211 input contained greater low frequency content, the value of Xu = -.025 was considered more accurate, though the sine wave input did attain R^2 and F-ratio values roughly twice as large as those for the 3211 input. This, however, was caused by the discrete, high frequency sine wave input strongly identifying Xw and Xq, but poorly identifying the low frequency effect, Xu. Still, the estimation of Xu = -.025 appeared low compared to the values produced by the 160 KCAS identification. These values ranged from $-.041 < Xu < -.021$. Since Xu

Table 7

200 KCAS Longitudinal Force and Moment Coefficients

Test Input	Xu	Xw	Xq	X_{HT}	R^2	F-Ratio	NDP
3211 Sine Wave	-.0250	.0160	1.37	.211	.1760	85.3	1600
	-.0066	.0211	.940	.179	.3626	227	1600
	Zu	Zw	Zq	Z_{HT}	R^2	F-Ratio	NDP
3211 Sine Wave	-.188	-.828	-7.37	-2.16	.9998	1.69×10^6	1600
	-.169	-.808	-3.14	-1.40	.9997	1.36×10^6	1600
	Mu	Mw	Mq	M_{HT}	R^2	F-Ratio	NDP
3211 Sine Wave	.0009	-.0101	-2.04	-.439	.9886	3.46×10^4	1600
	.0012	-.0092	-2.00	-.423	.9870	3.03×10^4	1600

represents an aerodynamic damping term, its absolute value should increase with airspeed.

To determine the effect that the parameter Xu had on longitudinal dynamics, a root locus plot was constructed. It was found that the change in Xu had a negligible effect on the short period roots, so the root locus, presented in Figure 12, shows only the variation in the phugoid eigenvalues as Xu varies from $-0.10 < Xu < 0.0$. Over the range $-.060 < Xu < -.025$, there was an 86% change in the real

part of the phugoid root, representing a significant change in phugoid damping.

Because of this large change in damping and because of the relatively small values of Xu produced by the preliminary identification, additional simulation runs were made. These runs consisted of 3211 horizontal tail inputs, similar to the previous inputs, but utilizing smaller stick deflections in an attempt to better excite the low frequency phugoid motion, and hence more accurately determine Xu.

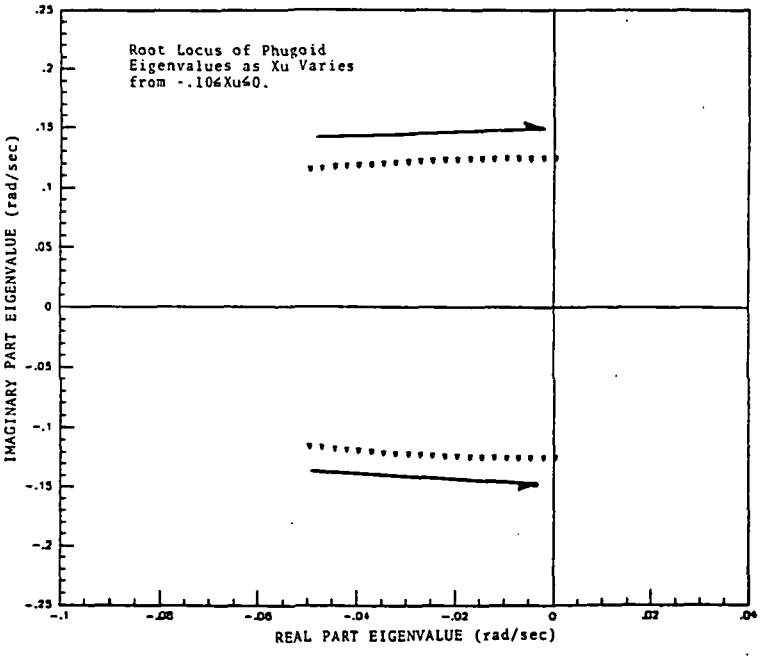

Figure 12

Root Locus of Phugoid Eigenvalues
With Variation of Xu

Table 8 shows that Xu was identified at a maximum of -.0437 with the 4% stick deflection. This affirmed that the actual value of Xu was in fact greater than those previously identified. Therefore, the final value of Xu was set at -.045, providing both reasonable damping and proper airspeed trends.

Table 8

Variation of Xu With Longitudinal Stick Deflection

Longitudinal Stick Deflection (%)	Xu	R^2	F-Ratio
3.0	-.0400	.219	224
4.0	-.0437	.201	201
5.0	-.0394	.192	94.7
7.0	-.0250	.176	85.2

Similarly, the other longitudinal parameters were determined by comparing statistical information, dynamic response characteristics and the root loci of parameters with a knowledge of fixed wing dynamics.

The final longitudinal model for the 200 KCAS identification, along with its eigenvalues and eigenvectors, is presented in Table 9. The final longitudinal results for the 160 KCAS simulation-produced linear model are shown in Table 10, and the final results for the 160 KCAS longitudinal flight data identification are presented in Table 11.

Table 9

Final 200 KCAS Longitudinal
Simulation Results

$$F = \begin{bmatrix} -.045 & .020 & 0.00 & -32.2 \\ -.185 & -.810 & 390. & .565 \\ .001 & -.010 & -2.01 & 0.00 \\ 0 & 0 & 1.00 & 0 \end{bmatrix} \quad x = \begin{bmatrix} u \\ w \\ q \\ \phi \end{bmatrix}$$

$$G = \begin{bmatrix} .200 \\ -2.00 \\ -.431 \\ 0 \end{bmatrix} \quad u = \begin{bmatrix} \delta_{HT} \end{bmatrix}$$

	Short Period Mode	Phugoid Mode
Eigenvalues:	$-1.41 \pm 1.88i$	$-.022 \pm .123i$
Eigenvectors:	$\begin{bmatrix} .0195 \pm .010i \\ 1.000 \\ -.0015 \pm .0048i \\ .0020 \pm .0007i \end{bmatrix}$	$\begin{bmatrix} 1.000 \\ .0037 \pm .0052i \\ .0005 \\ -.0007 \pm .0038i \end{bmatrix}$

Table 10

Final 160 KCAS Longitudinal
Simulation Results

$$F = \begin{bmatrix} -.040 & .056 & 0 & -32.2 \\ -.200 & -.660 & 308. & -3.64 \\ .0008 & -.008 & -1.7 & 0 \\ 0 & 0 & 1 & 0 \end{bmatrix} \quad x = \begin{bmatrix} u \\ w \\ q \\ \theta \end{bmatrix}$$

$$G = \begin{bmatrix} -.160 \\ -1.34 \\ -.280 \\ 0 \end{bmatrix} \quad u = \begin{bmatrix} \delta_{HT} \end{bmatrix}$$

	Short Period Mode	Phugoid Mode
Eigenvalues:	$-1.19 \pm 1.48i$	$-.0140 \pm .136i$
Eigenvectors:	$\begin{bmatrix} .0204 \pm .0013i \\ 1.000 \\ -.0017 \pm .0048i \\ .0025 \pm .0009i \end{bmatrix}$	$\begin{bmatrix} 1.000 \\ -.0246 \pm .002i \\ .0006 \pm .0001i \\ -.0009 \pm .0042i \end{bmatrix}$

Table 11

Final 160 KCAS Longitudinal
Flight Data Results

$$F = \begin{bmatrix} -.042 & .150 & 2.00 & -32.2 \\ -.120 & -.600 & 307. & -1.00 \\ .006 & -.010 & -3.00 & 0 \\ 0 & 0 & 1 & 0 \end{bmatrix} \qquad x = \begin{bmatrix} u \\ w \\ q \\ \theta \end{bmatrix}$$

$$G = \begin{bmatrix} -.070 \\ -.600 \\ .040 \\ 0 \end{bmatrix} \qquad u = \begin{bmatrix} \delta \\ XB \end{bmatrix}$$

	Short Period Mode	Phugoid Mode
Eigenvalues:	$-1.82 \pm 1.29i$	$-.0041 \pm .177i$
Eigenvectors:	$\begin{bmatrix} .0156 \pm .0252i \\ 1.000 \\ -.0040 \pm .0042i \\ .0025 \pm .0005i \end{bmatrix}$	$\begin{bmatrix} 1.000 \\ .302 \pm .0406i \\ .0010 \pm .0001i \\ -.0003 \pm .0057i \end{bmatrix}$

Tables 12 and 13 present the lateral force and moment derivatives along with R^2 and F-ratio values identified from the 200 KCAS aileron and rudder inputs respectively. For the 200 KCAS model identification, there were four separate preliminary models used to determine the final lateral model. In general, force and moment derivatives produced by rolling motion such as Yp were more strongly identified by the aileron input. Similarly, derivatives produced by yawing motion such as Lv were identified more strongly by the rudder input.

The parameter Lv was found to be particularly influential on the spiral mode. The root locus plot shown in Figure 13 illustrates this influence over the range $-.02 < Lv < .02$. Although the lowest value found by the identification was .0019, it is informative to plot this larger range which shows that the spiral mode becomes stable when $Lv < -.0069$.

Table 13 shows that the rudder-produced value of Lv was approximately .002 from both inputs. This value corresponds to a spiral root of 0.0636. The spiral roots for the four preliminary lateral models ranged from 0.059 to 0.065. Therefore, the final value of Lv was set to the rudder-produced value of 0.002.

The final 200 KCAS lateral linear model derived from the nonlinear simulation, along with its eigenvalues and eigenvectors, is shown in Table 14. The final 160 KCAS lateral results derived from the simulation are shown in

Table 15, and the results from the flight data identification at 160 KCAS are shown in Table 16.

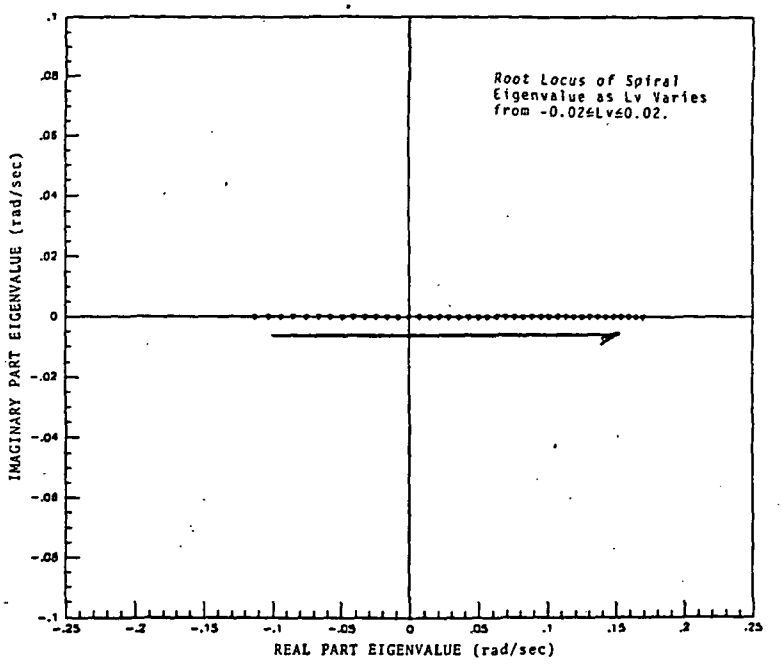

Figure 13

Root Locus of Spiral Eigenvalue
With Variation of Lv

Table 12

200 KCAS Lateral Force and Moment Coefficients From Aileron Input

Test Input	Yv	Yp	Yr	Y_{AIL}	R^2	F-Ratio	NDP
3211	-.164	-1.14	11.3	-.0051	.9945	7.15×10^4	1600
Sine Wave	-.249	-.605	4.50	0.000	.9999	2.44×10^7	1600

	Lv	Lp	Lr	L_{AIL}	R^2	F-Ratio	NDP
3211	.0178	-2.26	-1.12	.397	.9986	2.76×10^5	1600
Sine Wave	.0105	-2.26	.647	.405	.9979	1.92×10^5	1600

	Nv	Np	Nr	N_{AIL}	R^2	F-Ratio	NDP
3211	.0053	.101	-.917	-.0136	.9896	3.79×10^4	1600
Sine Wave	.0066	.0855	-1.23	-.0144	.9992	5.27×10^5	1600

Table 13

200 KCAS Lateral Force and Moment Coefficients From Rudder Input

Test Input	Yv	Yp	Yr	Y_{RUD}	R^2	F-Ratio	NDP
3211	-.249	0.	5.05	-.169	.9999	2.40×10^7	1600
Sine Wave	-.248	0.	5.11	-.170	.9999	1.86×10^7	1600

	Lv	Lp	Lr	L_{RUD}	R^2	F-Ratio	NDP
3211	.0021	-2.20	1.48	-.0215	.9657	1.12×10^4	1600
Sine Wave	.0019	-2.68	2.09	-.0325	.8302	1.95×10^3	1600

	Nv	Np	Nr	N_{RUD}	R^2	F-Ratio	NDP
3211	.0080	-.0677	-1.84	.0556	.9968	1.23×10^5	1600
Sine Wave	.0079	.197	-1.97	.0563	.9956	9.09×10^4	1600

Table 14

Final 200 KCAS Lateral Simulation Results

$$F = \begin{bmatrix} -.249 & 32.2 & -.700 & -388. \\ 0. & 0. & 1. & 0. \\ .002 & 0. & -2.26 & 1.65 \\ .008 & 0. & .090 & -1.90 \end{bmatrix} \qquad x = \begin{bmatrix} v \\ \phi \\ p \\ r \end{bmatrix}$$

$$G = \begin{bmatrix} 0. & -.169 \\ 0. & 0. \\ .400 & -.027 \\ -.014 & .056 \end{bmatrix} \qquad u = \begin{bmatrix} \delta_{AIL} \\ \delta_{RUD} \end{bmatrix}$$

	Dutch Roll Mode	Roll Subsidence Mode	Spiral Mode
Eigenvalues:	$-1.04 \pm 1.59i$	-2.39	.0636
Eigenvectors:	$\begin{bmatrix} 1.000 \\ -.0015 \pm .0016i \\ -.0010 \pm .0040i \\ .0019 \pm .0039i \end{bmatrix}$	$\begin{bmatrix} 1.000 \\ .0623 \\ -.149 \\ .0110 \end{bmatrix}$	$\begin{bmatrix} 1.000 \\ .0610 \\ .0039 \\ .0043 \end{bmatrix}$

Table 15

Final 160 KCAS Lateral
Simulation Results

$$F = \begin{bmatrix} -.210 & 31.9 & -1.20 & -310. \\ 0. & 0. & 1. & 0. \\ -.0055 & 0. & -1.94 & 1.65 \\ .0060 & 0. & .070 & -1.00 \end{bmatrix} \quad x = \begin{bmatrix} v \\ \phi \\ p \\ r \end{bmatrix}$$

$$G = \begin{bmatrix} 0. \\ 0. \\ .270 \\ -.0073 \end{bmatrix} \quad u = \begin{bmatrix} \delta_{AIL} \end{bmatrix}$$

	Dutch Roll Mode	Roll Subsidence Mode	Spiral Mode
Eigenvalues:	$-.574 \pm 1.32i$	-2.03	.0334
Eigenvectors:	$\begin{bmatrix} 1.000 \\ .0003 \pm .0027i \\ -.0037 \pm .0012i \\ .0012 \pm .0040i \end{bmatrix}$	$\begin{bmatrix} 1.000 \\ .435 \\ -.885 \\ .0540 \end{bmatrix}$	$\begin{bmatrix} 1.000 \\ .0656 \\ .0022 \\ .0060 \end{bmatrix}$

Table 16

Final 160 KCAS Lateral
Flight Data Results

$$F = \begin{bmatrix} -.0017 & 31.9 & 0. & -307. \\ 0. & 0. & 1. & 0. \\ -.0005 & 0. & -3.63 & .900 \\ .0415 & 0. & 2.00 & -3.85 \end{bmatrix} \quad x = \begin{bmatrix} v \\ \phi \\ p \\ r \end{bmatrix}$$

$$G = \begin{bmatrix} -.018 & -.005 \\ 0. & 0. \\ .200 & 0. \\ -.003 & -.0182 \end{bmatrix} \quad u = \begin{bmatrix} \delta_{AIL} \\ \delta_{RUD} \end{bmatrix}$$

	Dutch Roll Mode	Roll Subsidence Mode	Spiral Mode
Eigenvalues:	$-1.67 \pm 2.90i$	-4.16	.0243
Eigenvectors:	$\begin{bmatrix} 1.000 \\ -.0004 \pm .0007i \\ -.0013 \pm .0024i \\ .0054 \pm .0094i \end{bmatrix}$	$\begin{bmatrix} 1.000 \\ .0055 \\ -.0230 \\ .0141 \end{bmatrix}$	$\begin{bmatrix} 1.000 \\ .118 \\ .0029 \\ .0122 \end{bmatrix}$

CHAPTER 4

Discussion of Results

Simulation Linear Model Validation

To establish the accuracy of the final linear models derived from the nonlinear simulation, a comparison of predicted aircraft dynamics obtained from both nonlinear simulation and linear model responses was performed. Predictions were made with both the 160 KCAS and the 200 KCAS linear models using a doublet input profile to obtain time histories of the aircraft's response. The doublet input was chosen to confirm that the final linear models would accurately predict aircraft dynamics resulting from input profiles other than those from which the models were derived. All response comparisons show only the predicted disturbance component about the trim condition.

The results of the 160 KCAS longitudinal comparison are shown in Figures 14 through 16. Figure 14 shows the predicted response of w resulting from the horizontal tail doublet. The comparison shows that the responses of the nonlinear simulation and the linear model are virtually identical, with differences in magnitude of less than 1.7%. Figure 15 shows the predicted response of q. Once again the responses of the simulation and the linear model are nearly identical, displaying less than 3.3% difference in magnitude. This excellent correlation verifies that the

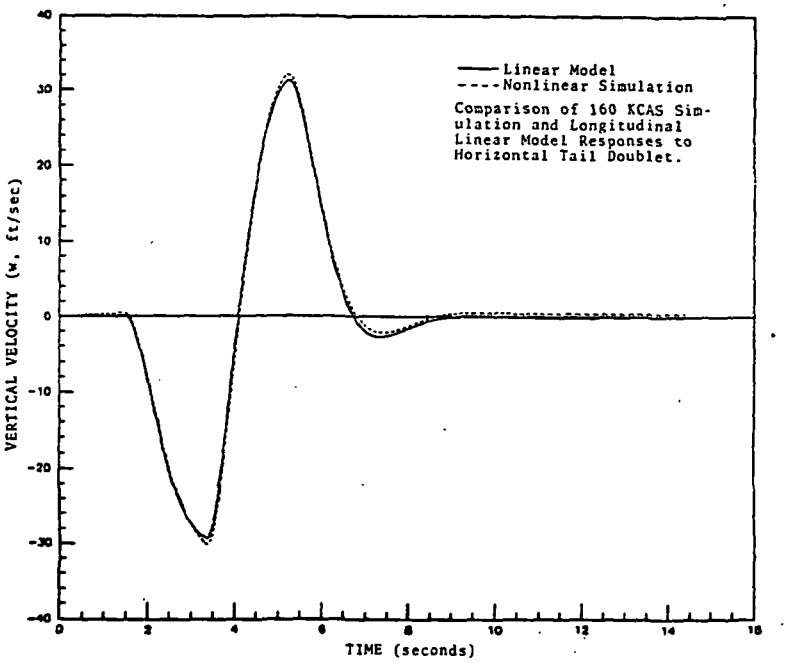

Figure 14

Comparison of 160 KCAS Simulation and Linear Model Responses of w

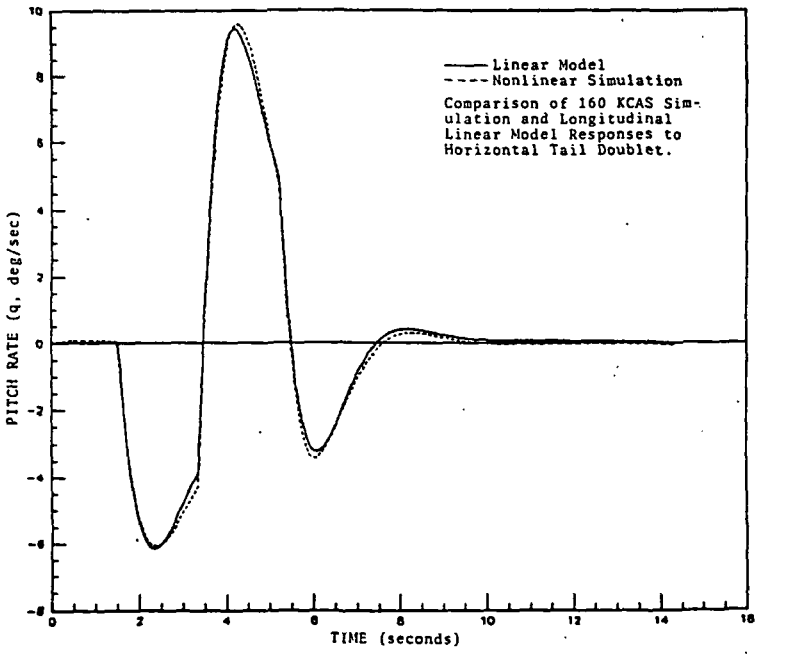

Figure 15

Comparison of 160 KCAS Simulation and Linear Model Responses of q

160 KCAS longitudinal linear model predicts short period dynamics with accuracy comparable to the nonlinear simulation.

Because of the long period of the phugoid mode (46.2 seconds), it was highly impractical and unfeasible to generate vehicle response time histories of this motion with the nonlinear simulation. Therefore, a direct comparison of the simulation and linear model phugoid responses is not available. However, for the intended purposes of the linear models which include pilot training and flight control law design, it is not necessary that the linear model phugoid response exactly match that of the nonlinear simulation. It is also not realistic to expect the two phugoid responses to be as well correlated as the short period motion was.

Figure 16 shows the first 15 seconds of the predicted response of u resulting from the horizontal tail doublet. This comparison shows that the linear model is slower to respond and not as sensitive to input as the nonlinear simulation, though generally the responses show similar dynamic trends. It is important to note here that even a difference of 10 ft/sec represents less than 3.25% difference relative to the trim value of u.

Since the parameter identification was performed over approximately a 20 second time history, the long period phugoid mode could not be fully identified because of incomplete dynamic information. Further, because there was

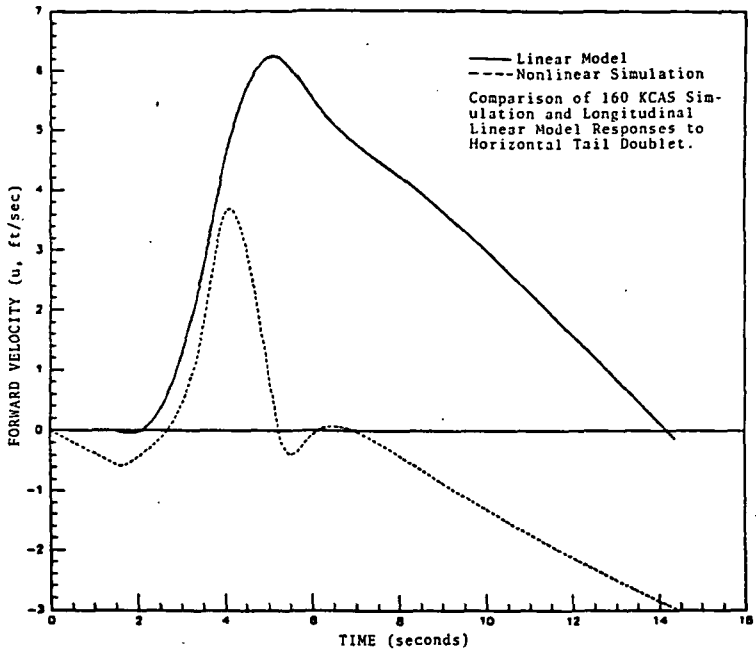

Figure 16

Comparison of 160 KCAS Simulation and Linear Model Responses of u

no thrust variation control as mentioned previously, ability to fully excite the phugoid motion was limited. Since the phugoid was found to be a very slow, stable motion, it can be easily controlled by either a pilot or an electronic flight control system, so the lack of an exact identification does not present any difficulties. Therefore, the linear model approximation of the phugoid response is adequate.

Overall the 160 KCAS longitudinal linear model is efficient in predicting dynamic trends and represents a valid alternative to the nonlinear simulation.

The results of the 160 KCAS lateral model validation comparisons are shown in Figures 17 and 18. Figure 17

shows the predicted response of p to an aileron doublet input. As expected, excellent correlation between the linear model response and the nonlinear simulation is evident. The maximum difference in magnitude is less than 9.5%. Figure 18 shows the response of r to the same aileron doublet. This comparison shows that r is well identified by the aileron input, even at low magnitudes ($r < 3.0$ deg/sec), with a difference in peak magnitudes of less than 9.4%.

These comparisons illustrate the effectiveness of the 160 KCAS lateral linear model in predicting the lateral dynamics of the RSRA. As with the longitudinal model, the efficiency of the lateral model is especially significant when the reduction in computational effort is considered.

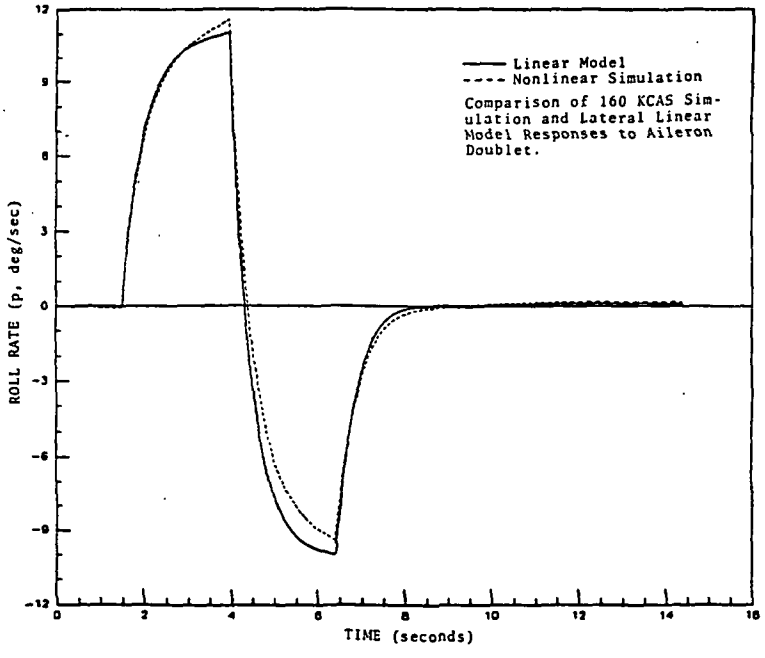

Figure 17

Comparison of 160 KCAS Simulation and Linear Model Responses of p

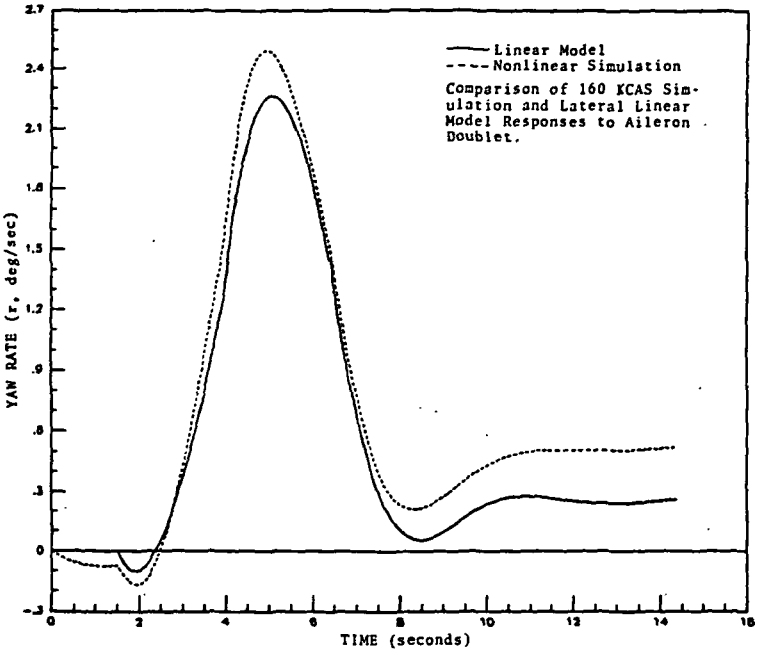

Figure 18

Comparison of 160 KCAS Simulation and Linear Model Responses of r

The results of the 200 KCAS longitudinal linear model validation are presented in Figures 19 and 20. Figure 19 shows the predicted response of w resulting from the 200 KCAS horizontal tail doublet. Like the 160 KCAS validation results, the 200 KCAS linear model and the nonlinear simulation produce almost identical predictions of w, with differences in magnitude less than 4.6%. Similarly, the comparison of predicted pitch rate response (q) shown in Figure 20 displays equally high correlation with differences less than 3.1%.

The 200 KCAS longitudinal linear model demonstrates accuracy equal to that of the nonlinear simulation in modeling short period dynamics. As was the case for the

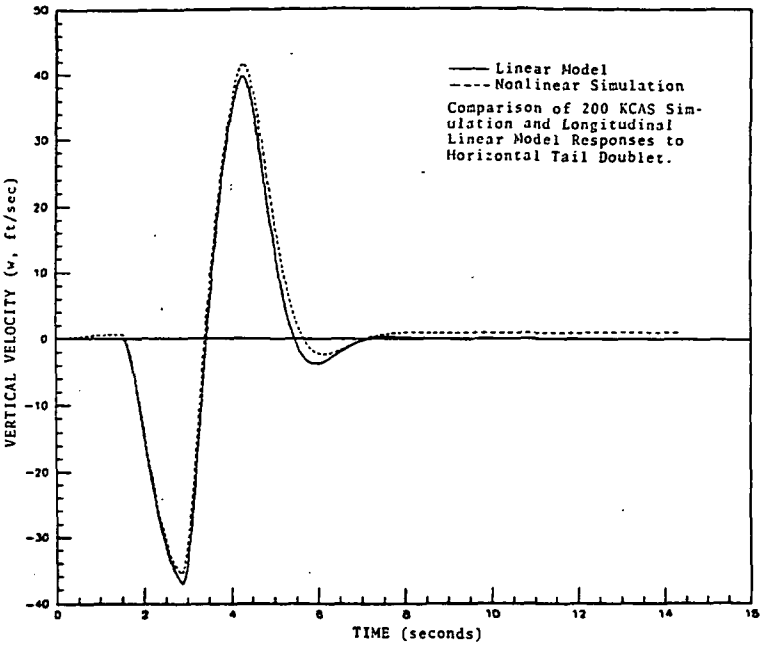

Figure 19

Comparison of 200 KCAS Simulation and Linear Model Responses of w

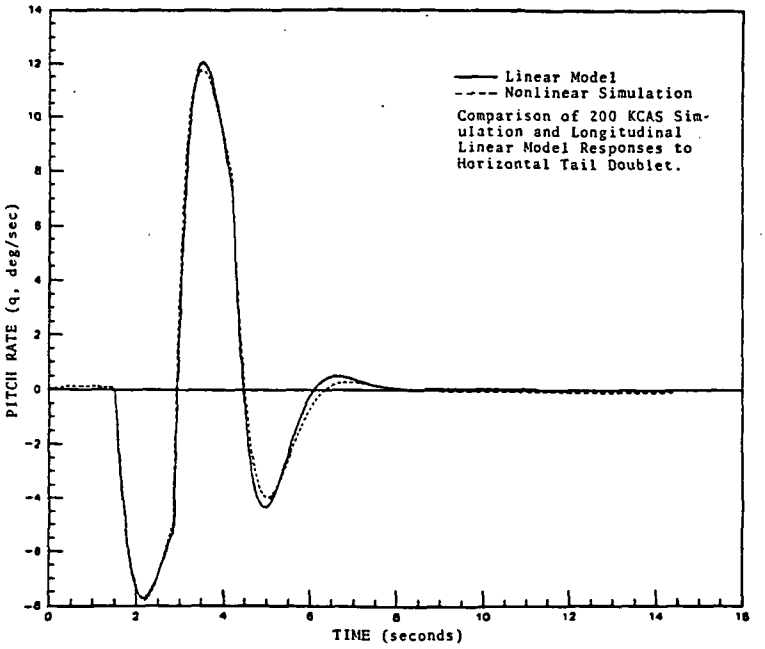

Figure 20

Comparison of 200 KCAS Simulation and Linear Model Responses of q

160 KCAS longitudinal model, the phugoid mode could not be fully identified for the reasons stated previously. But again at 200 KCAS, the phugoid mode is stable, has a period in excess of 51 seconds, and displays response trends similar to the nonlinear simulation which allows the linear model approximation to be used effectively. Therefore, the 200 KCAS longitudinal linear model can be used in place of the nonlinear simulation with similarly accurate dynamic predictions.

To establish the validity of the 200 KCAS simulation-derived lateral linear model, both aileron and rudder doublet inputs were evaluated. Figures 21 to 24 present the results of these comparisons. In general, the linear model predicted overall responses very similar to those of the nonlinear simulation when responding to the same axis inputs. This can be seen in Figure 21, displaying differences of less than 2.3% in roll rate response to the aileron input, and Figure 24 with differences also less than 2.3% in yaw rate response to the rudder input. The off axis responses of the linear model demonstrate similar dynamic trends compared with the simulation, but differ slightly in magnitude. These effects are seen in Figure 22, indicating an 8.3% maximum difference in predicted yaw rate response to the aileron input, and Figure 23, where a maximum 12.5% difference in predicted roll rate response to rudder input is observed. However, the overall magnitudes

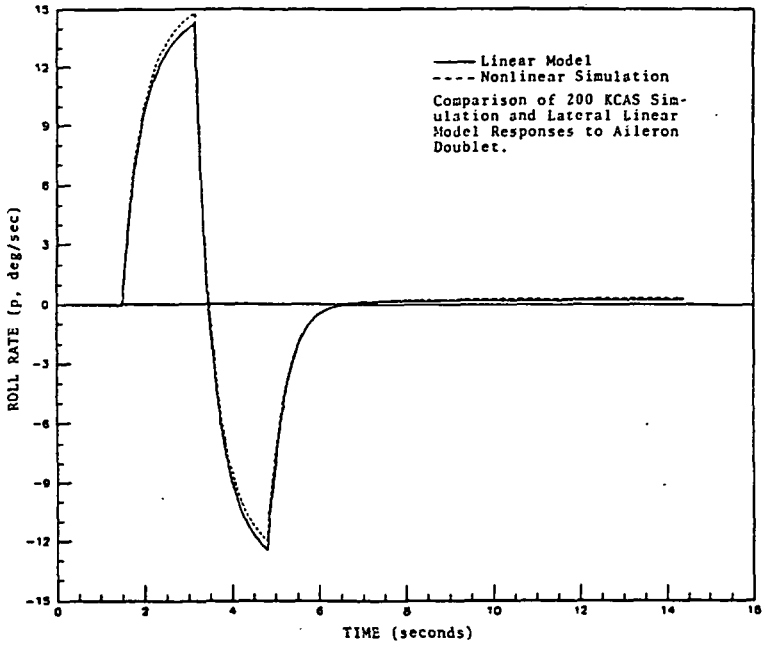

Figure 21

Comparison of 200 KCAS Simulation and Linear Model Responses of p

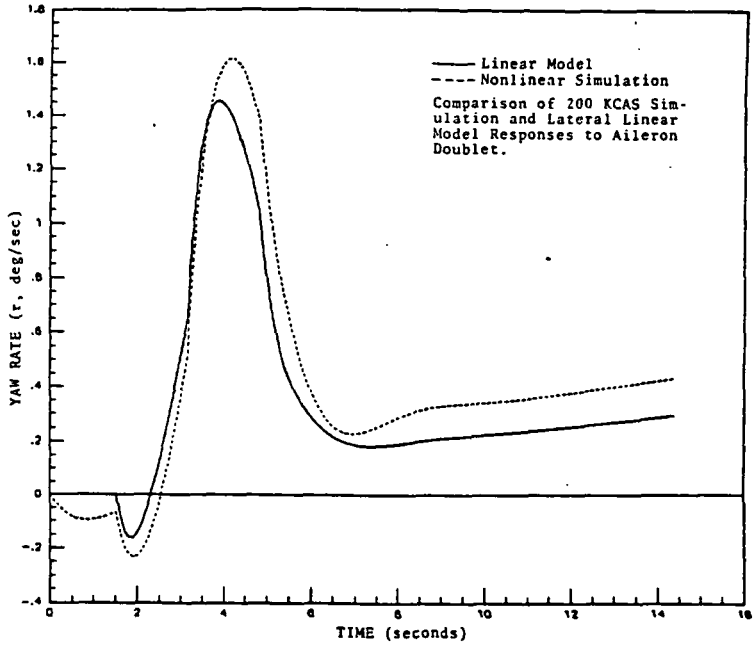

Figure 22

Comparison of 200 KCAS Simulation and Linear Model Responses of r

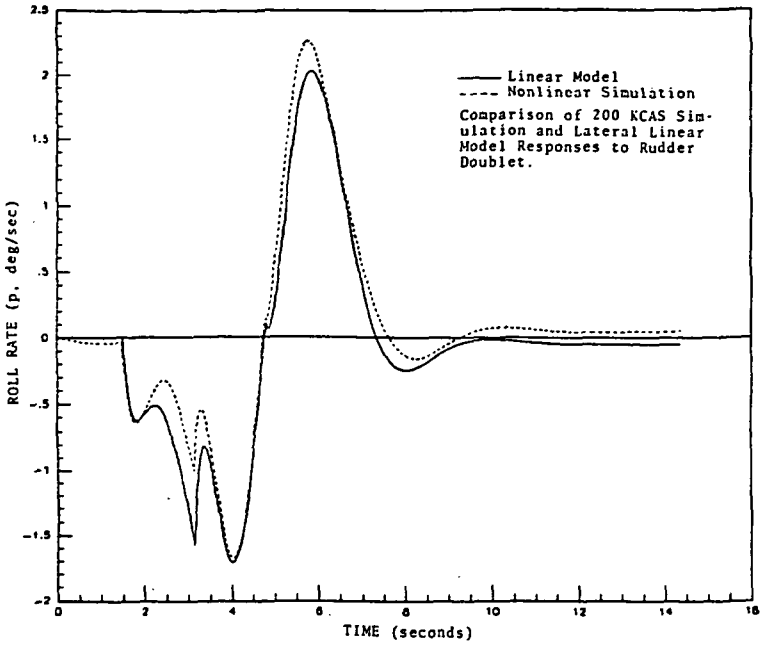

Figure 23

Comparison of 200 KCAS Simulation and Linear Model Responses of p

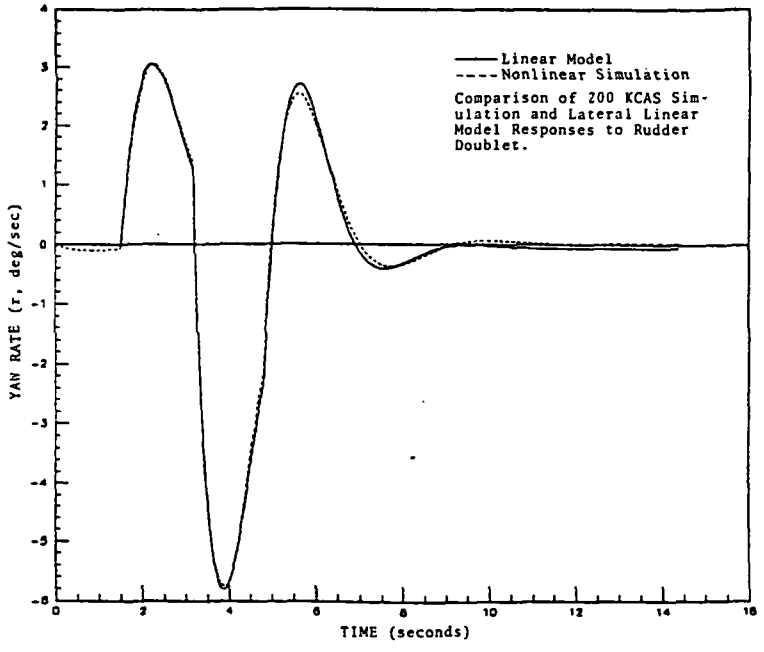

Figure 24

Comparison of 200 KCAS Simulation and Linear Model Responses of r

of the off axis disturbances are less than ± 2.5 deg/sec, thus they are small enough that the slight differences between the linear model and simulation become inconsequential. So the 200 KCAS lateral linear model has been shown to be highly effective in predicting lateral dynamics of the RSRA fixed wing aircraft.

In general it has been observed that all four linear models identified from the nonlinear simulation were highly effective in predicting aircraft dynamics. All four identified models produced very similar response trends, and differed only slightly in magnitude of response when compared to the simulation. These results are most impressive when the simplicity of the linear model structure is taken into account. The high degree of correlation demonstrated between the linear model and simulation dynamic responses verified that the decoupled, linearized, rigid body equations of motion form an extremely accurate dynamic model for predicting small disturbances of a symmetric aircraft about steady flight conditions. Further, each of the identified linear models have been validated for the RSRA fixed wing configuration at the specified flight conditions, and can thus be used with a high degree of confidence, with substantially less computational effort than required for the GENHEL nonlinear simulation.

Variation of Rigid Body Dynamics With Airspeed

With the validity of the simulation-derived linear models established, the variation of rigid body dynamics as airspeed increased from 160 KCAS to 200 KCAS was examined.

The effects of airspeed on the longitudinal dynamics are shown in Table 17. As shown in Table 17, the major effects of the increase in airspeed on the short period mode were a 23.7% increase in the undamped natural frequency, and a 15.5% decrease in time to damp to half amplitude. Thus as airspeed increased, the short period motion became faster and decayed quicker.

The most dramatic effect of increased airspeed on the phugoid mode was a 72.5% increase in damping ratio. This very large increase in damping was brought about by a 57.0% decrease in the value of the real part of the phugoid roots, which also reduced the time to half amplitude by 36.4%. Thus as airspeed increased, the phugoid mode became much more damped and the motion slowed slightly.

Also shown in Table 17 is the effect of airspeed on the resistance derivatives Xu, Zw and Mw, and the pitch damping term Mq. In general, the resistance derivatives and damping terms should increase numerically as airspeed increases and this effect is verified by the results shown in Table 16. The speed brake term Xu, which contributes heavily to the phugoid damping, increased numerically by 12.5%. The vertical resistance derivative Zw and the pitch

Table 17

Effect of Airspeed on
Longitudinal Dynamics

	160 KCAS	200 KCAS	Change (%)
Short Period Motion:			
Roots:	$-1.19 \pm 1.48i$	$-1.41 \pm 1.88i$	--
$t_{1/2}$, sec:	0.58	0.49	-15.5
$\frac{\text{rad}}{W_n}$, sec:	1.90	2.35	23.7
z:	.625	.600	-4.00
Phugoid Motion:			
Roots:	$-.014 \pm .136i$	$-.022 \pm .123i$	--
$t_{1/2}$, sec:	49.5	31.5	-36.4
$\frac{\text{rad}}{W_n}$, sec:	.137	.125	-8.80
z:	.102	.176	72.5
Longitudinal Derivatives:			
Xu:	-.040	-.045	-12.5
Zw:	-.660	-.810	-22.7
Mq:	-1.70	-2.01	-18.2
Mw:	-.008	-.010	-25.0

damping term Mq both increased numerically by 22.7% and 18.2% respectively. The resistance derivative Mw is directly proportional to M_{α}, the longitudinal static stability term. The results show that Mw was negative, as required, and increased numerically by 25.0% as airspeed increased. This indicates that in the fixed wing configuration, the longitudinal static stability of the RSRA increases with airspeed.

The effects of increased airspeed on the lateral dynamics are shown in Table 18. The primary effect of increased airspeed on the Dutch Roll mode was a decrease in time to half amplitude of 44.6%. This was caused by an 81.2% decrease in the real part of the Dutch Roll eigenvalues. The damping ratio and the undamped natural frequency also increased, by 37.0% and 31.9% respectively, as airspeed increased. One major reason for this dramatic change in the decay time can be seen by examining the preliminary lateral results for the 200 KCAS identification. The real parts of the Dutch Roll eigenvalues produced by the aileron and rudder inputs were significantly different, as seen in Table 19.

The results in Table 19 show that, as expected, the Dutch Roll mode was much more sensitive to rudder input than to aileron input. Therefore, in order to obtain a complete identification of Dutch Roll characteristics, it is necessary to use both aileron and rudder inputs.

The roll subsidence mode, as shown in Table 18, decayed much more quickly as airspeed increased. The eigenvalue decreased by 17.7%, which led to a 14.7% decrease in time to half amplitude. At both airspeeds, the roll subsidence mode decayed so rapidly that it is of little consequence to the overall lateral dynamics.

In contrast to the roll subsidence mode, the spiral mode is critical to the lateral dynamics of the aircraft. The spiral mode was found to be unstable and became less

Table 18

Effect of Airspeed on
Lateral Dynamics

	160 KCAS	200 KCAS	Change (%)
Dutch Roll Motion:			
Roots:	$-.574 \pm 1.32i$	$-1.04 \pm 1.59i$	--
$t_{1/2}$, sec:	1.21	0.67	-44.6
W_n, $\frac{rad}{sec}$:	1.44	1.90	31.9
z:	.400	.425	37.0
Roll Subsidence:			
Root:	-2.03	-2.39	-17.7
$t_{1/2}$, sec:	0.34	0.29	-14.7
Spiral Mode:			
Root:	.0334	.0636	90.4
t_2, sec:	20.8	10.9	-47.6
Lateral Derivatives:			
Lv:	-.0055	.0020	136.
Lp:	-1.94	-2.26	-16.5
Nr:	-1.00	-1.90	-90.0
Nv:	.006	.008	33.3

Table 19

Variation of Real Part of Dutch Roll
Eigenvalues With Control Input

Control Input	Aileron	Rudder	Change %)
Sine Wave	-.740	-1.02	-37.6
3211	-.568	-1.09	-91.2

stable as airspeed increased. The time to double amplitude decreased by 47.6% due to the 90.4% increase of the spiral eigenvalue. The fact that the mode is unstable, with a time to double of less than 11.0 seconds at 200 KCAS, requires that active pilot control or a stability augmentation system be operative at all times.

The decrease in stability of the spiral mode as speed increased was caused mainly by the increase in the parameter Lv. Lv, which was shown previously to dramatically affect the spiral divergence, increased by 136%, changing sign from negative to positive. At small angles of attack, Lv is proportional to L_β, the lateral static stability derivative. Therefore, as speed increases the lateral static stability (dihedral effect) decreases and becomes destabilizing. This is not the case for the directional static stability, however, as Nv, which is proportional to N_β (weathervane effect), increased by 33.3% adding directional stability as speed increased.

As expected, the damping terms Lp and Nr increased numerically with airspeed. Lp, which is roughly equivalent to the roll subsidence eigenvalue, increased by 16.5%. Nr increased numerically by 90.0% as airspeed increased, but some of this increase was likely caused by not having used a rudder input for the 160 KCAS simulation lateral linear model identification.

Flight Data Linear Model Validation

To establish the validity of the linear models derived from flight data at 160 KCAS, the predicted dynamic responses were compared with the actual (flight data) responses.

Figure 25 shows the flight data linear model predicted response of q compared to the actual aircraft response for a horizontal tail 2311 input. Considering the simplicity of the linear model, the high correlation of the two responses is most impressive. The linear model does differ in magnitude from the actual data by as much as 27.0%, but generally the two responses display similar dynamic trends. Thus the longitudinal linear model derived from flight data provides accurate dynamic trends at a small fraction of the time and expense it takes to measure and record reliable flight data with the RSRA.

Figures 26 and 27 present the results of the lateral linear model predictions. Figure 26 displays the linear model predicted response of p to an aileron sine sweep maneuver, along with the actual response. This comparison indicates that the linear model substantially under-predicts the low frequency response of the roll rate. But as the frequency of the motion approaches 3.0 rad/sec (near t = 62 sec), the linear model and the actual data differ by no more than 24.0%. Similarly, in Figure 27, which displays the yaw rate response to a rudder sine sweep maneuver, it is again seen that the linear model and flight

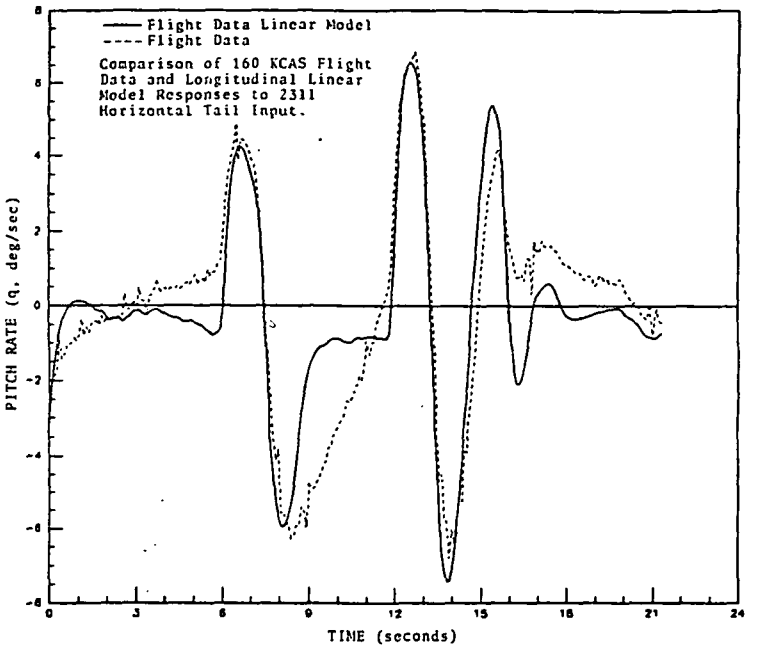

Figure 25

Comparison of Flight Data and
Linear Model Responses of q

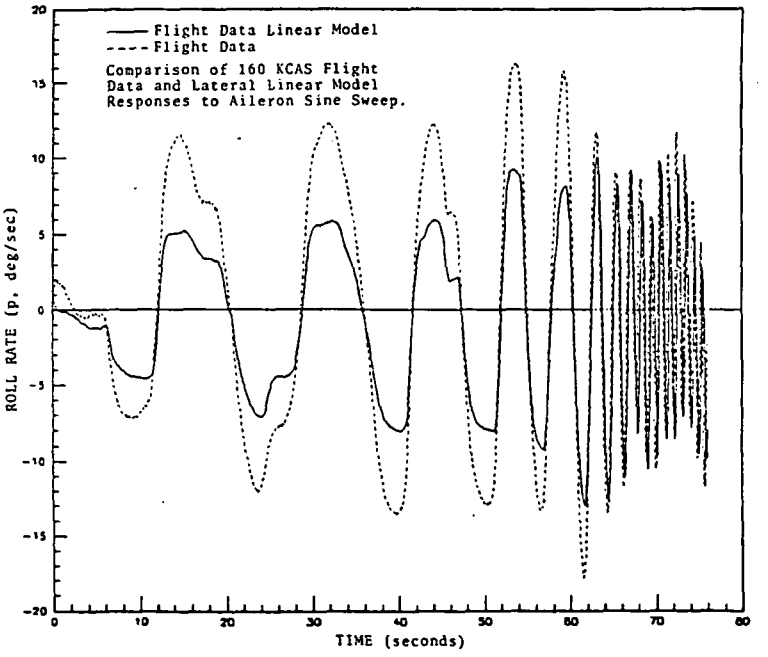

Figure 26

Comparison of Flight Data and
Linear Model Responses of p

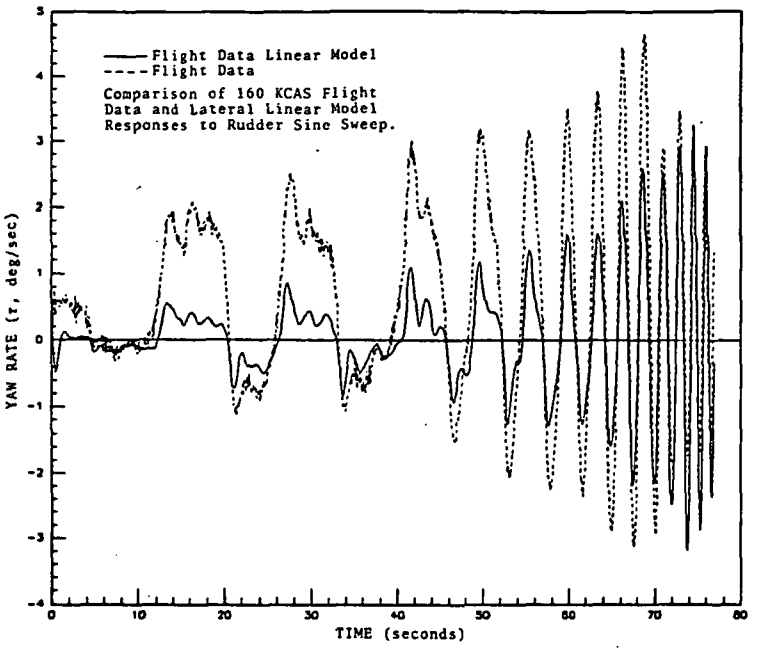

Figure 27

Comparison of Flight Data and Linear Model Responses of r

data become better correlated at frequencies above 3.0 rad/sec. Above this frequency, the differences in magnitude become less than 25.0%. Not surprisingly, the undamped natural frequency of the Dutch Roll mode produced by the flight data linear model was found to be 3.35 rad/sec, approximately the same frequency at which the lateral linear model becomes much more accurate. More importantly, in both the aileron and the rudder sine sweep comparisons, the linear model tracks the dynamic trends of the flight data responses, and produces no apparent phase shift. Therefore, the lateral linear model derived from flight data provides accurate dynamic information quickly and effectively.

Overall, the flight data derived linear models are efficient in providing insight to the dynamic response of the aircraft, and provide a fast, inexpensive alternative to a fully instrumented flight test.

Comparison of Flight Data and Simulation Results

The final objective of this report was to compare, both qualitatively and quantitatively, the flight data-derived linear models with the nonlinear simulation produced linear models at 160 KCAS, and determine the similarities and differences between the two. To accomplish this qualitatively, the validation comparisons performed previously for both simulation and flight data linear models were recreated. To the simulation-derived linear model validations, the flight data linear model responses were added. To the flight data linear model validations, the simulation linear model responses were added. In this way the dynamic responses of both sets of linear models could be compared directly and against the baseline (either nonlinear simulation or flight data).

The simulation validation response plots with the flight data linear model responses added are shown in Figures 28 and 29. Figure 28 presents the comparison of predicted pitch rate responses resulting from the horizontal tail doublet. This comparison illustrates the remarkable correlation of both longitudinal linear models with the nonlinear simulation response. The flight data

linear model and the simulation linear model responses are both within 10.0% in magnitude of the nonlinear simulation response, and all three share nearly identical dynamic shapes. This confirms that the two longitudinal linear models, identified with separate dynamic information, do in fact produce comparable predictions of RSRA rigid body motion.

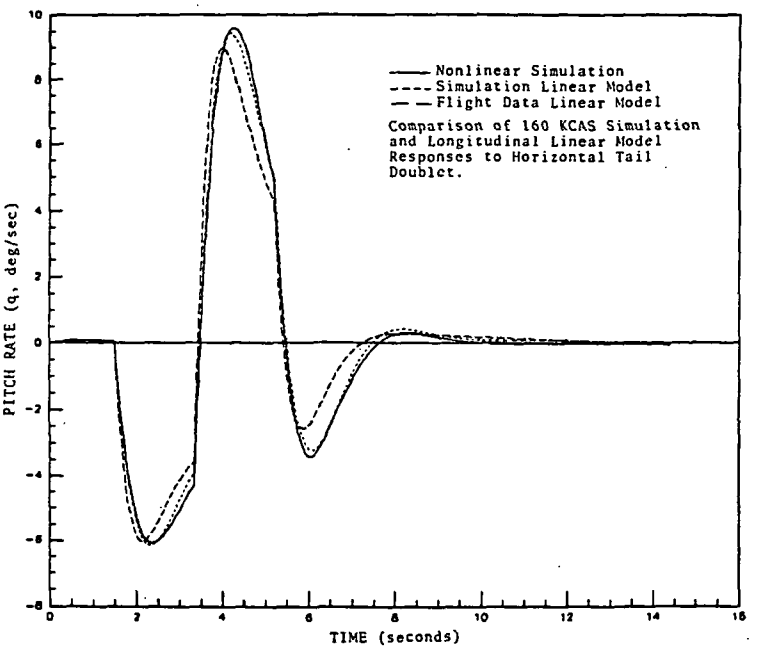

Figure 28

Comparison of Longitudinal Linear Model and Simulation Responses of q

Figure 29 presents the comparisons of predicted roll rate responses resulting from the aileron doublet input. In this comparison the roll rate response of the flight data lateral linear model rises very quickly, approximating a first order response. In fact, this response is caused mainly by the heavily damped roll subsidence mode, which

was found to have an eigenvalue of -4.16 rad/sec. The flight data linear model is within 2.0% of its steady state value less than one second after the command input. This is the same response that the roll subsidence mode of the flight data linear model predicts. Though the magnitude of the flight data linear model response is about 60.0% less than that of the nonlinear simulation, the important aspect is that both linear model responses display the same dynamic trends. The magnitude of the flight data linear model response could be increased by altering the G matrix, making the model more sensitive to input, if an application required greater magnitude correlation. This is true, of course, for the other linear models as well, but this must

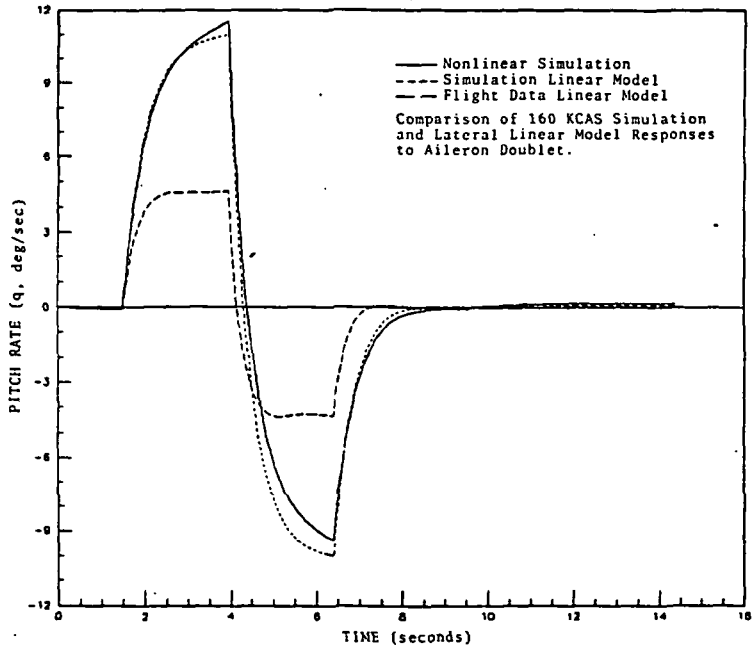

Figure 29

Comparison of Lateral Linear Model and Simulation Responses of p

be done carefully, since it affects all control inputs used, and may result in unrealistic dynamic responses.

Therefore it is evident that the two identified lateral linear models produce similar dynamic predictions, though the flight data linear model displays much faster response. The faster response of the flight data linear model is likely due in part to the addition of the tail rotor.

Figures 30 and 31 present the flight data validation comparisons with the predicted responses of the simulation linear models added. Figure 30 displays the responses of the pitch rate (q) produced by the horizontal tail 2311 input. This comparison shows that the simulation- and flight data-derived longitudinal models respond almost identically, with maximum differences in magnitude of less than 10.3% between the two model responses. Again this verifies that, although they were identified with different dynamic information, the two longitudinal linear models produce very similar response predictions.

Figure 31 shows the response of the roll rate (p) to an aileron sine sweep maneuver. In contrast to the flight data-derived linear model, the simulation linear model overpredicts the magnitude of response at low frequencies. This effect is most evident at negative (right wing up) roll rates. This trend continues even at higher frequencies where the flight data linear model becomes more accurate. The fact that the simulation lateral linear

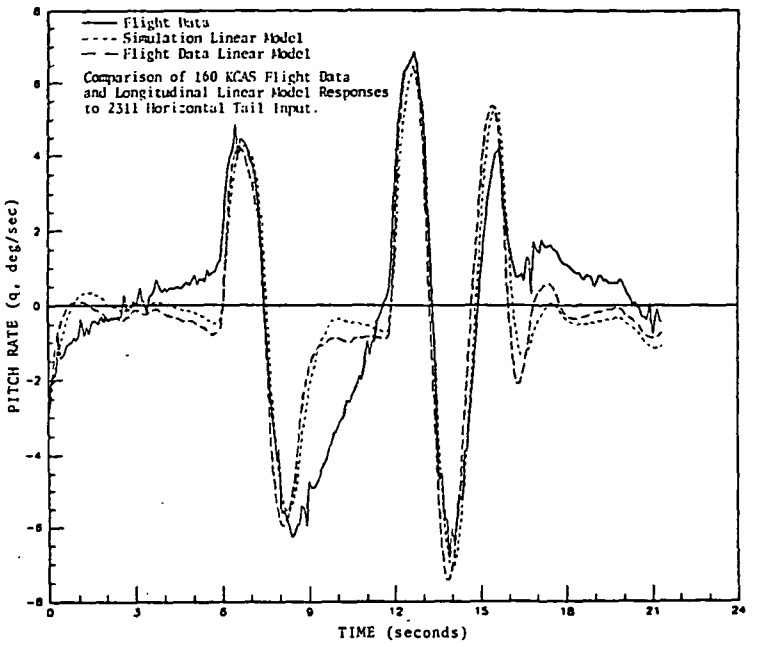

Figure 30

Comparison of Longitudinal Linear Model and Flight Data Responses of q

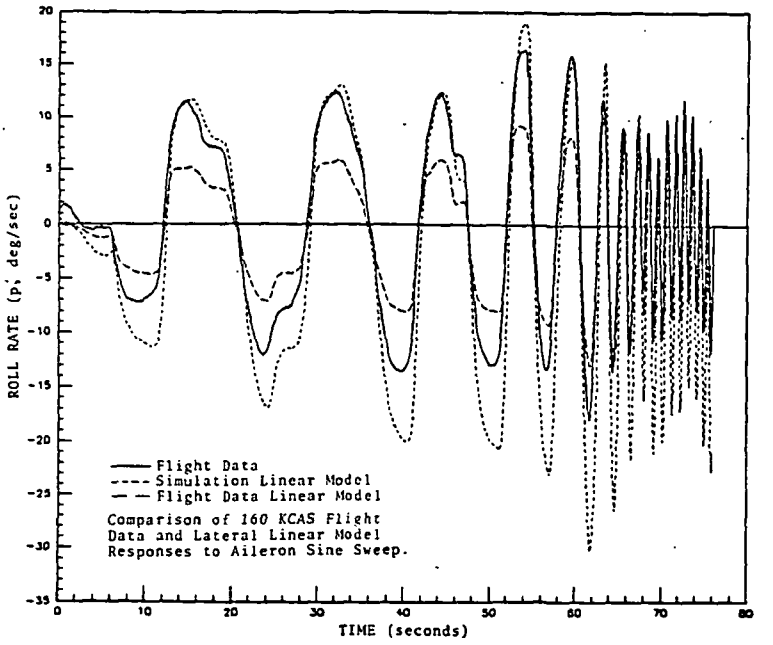

Figure 31

Comparison of Lateral Linear Model and Flight Data Responses of p

model response overpredicted primarily right-wing-up motion indicates that there is some asymmetry that the flight data and hence the flight data linear model detect, but is not modeled by the simulation linear model.

When viewing the RSRA, it is evident that the tail rotor is above the roll axis of the aircraft, and thus introduces rolling moments. The simulation identification, completed prior to flight testing, was accomplished without the tail rotor present. As previously mentioned, however, the tail rotor was left installed for flight testing but was not used for control purposes once airborne. The tail rotor was rotating at zero installed pitch and at normal speed (1243 RPM) throughout the flight tests. Thus when the aircraft rolls positively, the vertical tail blocks the side velocity from the tail rotor, reducing the roll damping effects of the tail rotor. However, when the aircraft rolls negatively, both the tail rotor and the vertical tail are exposed to side velocity imposed by the roll rate and an increase in roll damping is experienced. These phenomena explain, in part, why the simulation lateral linear model, identified without tail rotor effects, overpredicts the maximum negative roll rates of the aircraft.

Overall, considering that the nonlinear simulation and flight test trim conditions and aircraft configurations were not identical, the predicted responses of the identified linear models produce very impressive correlation.

The simulation- and flight data-produced longitudinal linear models have been shown to predict very accurate dynamic behavior compared to either the nonlinear simulation or actual flight data. The response predictions of the identified lateral linear models were not as well correlated as the longitudinal models, but still provided accurate information concerning dynamic trends of the aircraft. Only when these results are viewed with respect to their simplicity do the linear models become invaluable as a tool for predicting RSRA rigid body dynamics.

To better illustrate the quantitative differences between the simulation and flight data linear models, comparisons of the rigid body modes and selected stability derivatives were made. The results of the longitudinal dynamic comparison are shown in Table 20, and the lateral dynamic comparisons are shown in Table 21.

As seen in Table 20, the time to half amplitude of the short period mode produced by the flight data linear model was 34.5% less than that of the simulation linear model. The damping ratio of the flight data model was 30.4% greater than that of the simulation model. So, in general, the short period motion predicted by the flight data linear model decayed faster and was more heavily damped than the simulation linear model predicted.

In contrast to the short period mode, the phugoid motion predicted by the flight data linear model displayed significantly less damping than predicted by the simulation

Table 20

Comparison of Simulation and Flight Data
Linear Model Longitudinal Dynamics

	Simulation Linear Model	Flight Data Linear Model	Change (%)
Short Period Motion:			
Roots:	$-1.19 \pm 1.48i$	$-1.82 \pm 1.29i$	--
$t_{1/2}$, sec:	0.58	0.38	-34.5
W_n, rad/sec:	1.90	2.23	17.4
z:	.625	.815	30.4
Phugoid Motion:			
Roots:	$-0.14 \pm .136i$	$-.0041 \pm .177i$	--
$t_{1/2}$, sec:	49.5	169	241
W_n, rad/sec:	.137	.177	29.2
z:	.102	.0233	-77.2
Longitudinal Derivatives:			
Xu:	-.040	-.042	-5.00
Zw:	-.660	-.600	9.10
Mq:	-1.70	-3.00	-76.5
Mw:	-.008	-.010	-25.0

Table 21

Comparison of Simulation and Flight Data
Linear Model Lateral Dynamics

	Simulation Linear Model	Flight Data Linear Model	Change (%)
Dutch Roll Motion:			
Roots:	-.574 ± 1.32i	-1.67 ± 2.90i	--
$t_{1/2}$, sec:	1.21	.42	-65.3
W_n, $\frac{rad}{sec}$:	1.44	3.35	133.
z:	.400	.500	25.0
Roll Subsidence:			
Root:	-2.03	-4.16	-105.
$t_{1/2}$, sec:	.34	.16	-52.9
Spiral Mode:			
Root:	.0334	.0243	-27.2
t_2, sec:	20.8	28.5	37.0
Lateral Derivatives:			
Lv:	-.0055	-.0005	90.9
Lp:	-1.94	-3.63	-87.1
Nr:	-1.00	-3.85	-285.
Nv:	.006	.008	33.3

linear model. The time to half amplitude of the flight data model was 241% larger, and the damping ratio was 77.2% less overall. Therefore, the phugoid motion predicted by the flight data linear model was slightly faster, but decayed much more slowly when compared to the simulation linear model.

As shown in Table 20, the resistance derivatives Xu and Zw were approximately the same for both the simulation and flight data linear models. The pitch damping term Mq was significantly greater in magnitude (76.5%) for the flight data linear model. It was also observed that the longitudinal static stability was 25.0% greater for the flight data linear model.

As seen in Table 21, the Dutch Roll mode predicted by the flight data linear model had a natural frequency 133% greater than that predicted by the simulation model, and a half life 65.3% less. The flight data model also predicts a 25.0% higher damping ratio. Thus the Dutch Roll mode obtained with the flight data linear model was faster and decayed much more quickly compared to the simulation linear model.

As discussed previously, the roll subsidence mode was found to decay much more quickly with the flight data linear model. The eigenvalue of the mode was 105% greater for the flight data linear model than for the simulation linear model. The roll subsidence mode predicted by the flight data model decays so quickly, as seen in the

response comparisons, that it is of no consequence to the lateral dynamics.

The spiral mode was found to be less unstable with the flight data linear model than the simulation model. The spiral eigenvalue identified by the flight data model was 27.2% less than that predicted by the simulation linear model, increasing the time to double amplitude by 37.0%, or to almost 30 seconds.

As shown in Table 21, the flight data linear model produces much greater values of the lateral damping derivatives than the simulation linear model. The value of Nr produced by the flight data linear model was 285% greater and the value of Lp was 87.1% greater than the values produced by the simulation linear model. The weathervane effect was found to be 33.3% greater for the flight data linear model, while the dihedral effect was found to be 90.9% less, but still stabilizing.

The foregoing quantitative results from the flight data-derived linear models indicate that there are no significant handling qualities problems present with the RSRA fixed wing configuration. The fast motions, the short period and Dutch Roll modes were found to be heavily damped and thus present no problems. The phugoid mode, although very lightly damped, is of such long duration that it is not detectable. The spiral divergence must be controlled, but the time to double amplitude is such that this is not a difficulty.

The differences in the natural dynamic modes predicted by the simulation and flight data linear models at 160 KCAS could be caused by several factors. The two factors which are believed to be the most influential are the variations in aircraft trim configuration and the control inputs used in the identification process.

Since the aircraft configuration used in the simulation was determined prior to actual flight testing, some fundamental differences between the simulation aircraft and the actual aircraft existed (see Appendixes A and B). These differences included the tail rotor control and variations in wing incidence and flap deflection settings. In addition to these differences, parameters such as the aircraft body axes moments of inertia are not precisely known. The combination of these variations in aircraft configuration could affect both the trim conditions of the aircraft and subsequent dynamic response to a control input. Thus, linear models identified with different trim configurations would reflect these variations in the natural dynamic modes predicted. Specifically, the addition of the tail rotor during flight testing was responsible, in part, for the increased damping of the Dutch Roll and roll subsidence modes predicted by the flight data lateral linear model.

Probably the most influential factor affecting the identification of the linear models was the type of control input used in the identification process. As discussed in

Chapter 3, if the inputs do not contain the required energy and frequency content, the accuracy of the model identification will be reduced. Further, if the control inputs are not executed along the proper aircraft axes, model accuracy is also reduced. This effect is illustrated by the variations in the Dutch Roll decay rates. Since a rudder input was not used to identify the 160 KCAS simulation lateral linear model, the Dutch Roll mode could not be fully excited. The flight data linear model which was identified using both aileron and rudder sine sweeps predicted much faster transient decay than the simulation model. The use of a rudder input to identify the 160 KCAS simulation model would likely have produced significantly smaller (larger numerically) real parts of the Dutch Roll eigenvalues, similar to the 200 KCAS case shown in Table 19. Correspondingly, this would have produced quicker decay rates, and a higher correlation between the simulation and flight data linear model predicted dynamics.

The importance of the control input is also illustrated by the variations in the phugoid motion predicted by the 160 KCAS simulation and flight data longitudinal linear models. Since there was no control input that could directly excite the phugoid motion, it was more difficult to identify the fundamental characteristics of this motion. Thus the great disparity in damping ratio and time to half amplitude between the simulation and flight data linear models was not unexpected. However, it is clear from the

identification that the phugoid mode is stable and is of very long duration and therefore does not cause a problem with the overall aircraft dynamics.

It is evident, then, that with the selection of the proper dynamic input about the desired aircraft trim conditions, a highly accurate linear model representation of the actual aircraft dynamics can be achieved.

CHAPTER 5

Conclusions

In this report, system identification techniques were used to identify decoupled, linearized equations of rigid body motion for the fixed wing configuration of the RSRA. The linear models were established at 160 KCAS from both the GENHEL nonlinear simulation and from flight test data, and at 200 KCAS from the simulation.

Preliminary linear models obtained from the simulation were identified using 3211 and sine wave control input profiles at both airspeeds. Horizontal tail deflections were used to excite the longitudinal motion and aileron inputs were used to excite lateral motion. In addition, a rudder deflection was used for the 200 KCAS lateral model identification. Preliminary linear models obtained from flight test data at 160 KCAS were identified using 2311 and sine sweep control input profiles. Longitudinal motion was again excited with horizontal tail inputs, and lateral motion was excited by both aileron and rudder inputs.

The final linear models for each case were determined by examining statistical information, dynamic response characteristics and root loci of parameters, then correlating this information with an engineering knowledge of fixed wing aircraft dynamics.

To establish the accuracy of the final linear models, comparisons of predicted aircraft dynamics were performed. The results verified that the linear models obtained from the simulation were highly effective in predicting aircraft dynamic behavior at both 160 KCAS and 200 KCAS, and with substantially less computational effort than required by the nonlinear simulation. It was also shown that the linear models obtained from flight data were effective in providing insight to the actual dynamic response of the aircraft, and thus invaluable as a tool for pre-flight investigations.

Comparisons of the rigid body modes predicted by the simulation linear models at different airspeeds showed that, in general, the oscillatory modes decayed more quickly at the higher airspeed. The spiral motion was shown to become more unstable as airspeed increased. The comparisons also showed that longitudinal static stability and directional static stability increased with airspeed, while the lateral static stability became destabilizing at higher airspeed.

Comparisons of the flight data and simulation linear models at 160 KCAS showed that both models predict similar dynamic responses for the longitudinal case, but differ slightly in lateral responses, partially due to tail rotor effects. The flight data linear model indicated that no significant handling qualities problems are present in the

natural modes of the RSRA fixed wing configuration at 160 KCAS.

In summary, parameter identification utilizing the decoupled, linearized, rigid body equations of motion has been shown to provide accurate estimations of RSRA fixed wing dynamics with significantly reduced computational effort. The linear models obtained from both flight data and simulation have been shown to be valid alternatives to the nonlinear simulation, providing accurate predictions that can be used for pilot training purposes, flight control law design and stability and control evaluations.

In the future, it is recommended that linear models be obtained from flight data at 200 KCAS to confirm variations in rigid body dynamics with airspeed. It is also recommended that rudder inputs be used to identify all lateral linear models, and that variations in aircraft configuration and trim conditions be minimized, to improve the accuracy of the linear models and decrease the variations between the flight data and nonlinear simulation results.

List of References

1. Houck, J.A., et al, "Rotor Systems Research Aircraft Simulation Mathematical Model," NASA TM 78629, November 1977.

2. Schetzer, J., "Study Materials for Mechanics of Flight," California Polytechnic State University, San Luis Obispo, California.

3. DuVal, R.W., Wang, J.C., Demiroz, M.Y., "A Practical Approach to Rotorcraft Systems Identification," NASA Ames Research Center, Moffett Field, California, 1982.

4. Anon., "SCI Model Structure Determination Program (OSR) User's Guide," Systems Control Inc., Palo Alto, California.

5. Gupta, N.K., Hall, W.E., Trankle, T.L., "Advanced Methods of Model Structure Determination From Test Data," AIAA Guidance and Control Conference, Hollywood, Florida, August 1977.

6. Mohr, R.L., "DEKFIS 2 User's Guide: Discrete Extended Kalman Filter and Fixed Interval Smoother," Draft Report, Systems Control Inc., Palo Alto, California, June 1983.

Appendix A

Summary of 200 KCAS Simulation Trim Conditions

Wing Incidence:	7.5°
Flap Deflection:	0.0°
Gross Weight:	25,000 lb
Fuselage Station of CG:	302 in
Waterline Station of CG:	230.8 in
Tail Rotor:	off
Density Altitude:	10,000 ft
True Airspeed:	393 ft/sec
Pitch Attitude, θ:	-1.01°
Roll Attitude, Φ:	.027°
Wing Angle of Attack, α_w:	6.49°
Trim Value of Lateral Stick:	51.46% (100% = Full Right)
Trim Value of Longitudinal Stick:	49.38% (100% = Full Forward)
Trim Value of Pedals:	50.17% (100% = Full Right Pedal)

Appendix B

Summary of 160 KCAS Flight Test
Trim Conditions

Wing Incidence:	5.0°
Flap Deflection:	5.0°
Gross Weight:	25,712 lb
Fuselage Station of CG:	302 in
Waterline Station of CG:	230 in
Tail Rotor:	On, not controlled
Density Altitude:	9,500 ft
True Airspeed:	312 ft/sec
Pitch Attitude, θ:	1.5°
Roll Attitude, Φ:	0.7°
Wing Angle of Attack, α_w:	8.0°
Trim Value of Lateral Stick*:	52.3% (100% = Full Right)
Trim Value of Longitudinal Stick*:	46.7% (100% = Full Rearward)
Trim Value of Pedals*:	46.% (100% = Full Right Pedal)

*These are approximate control positions prior to a typical dynamic maneuver.

C-2

ABSTRACT

IDENTIFICATION OF LINEARIZED EQUATIONS OF MOTION FOR THE FIXED WING CONFIGURATION OF THE ROTOR SYSTEMS RESEARCH AIRCRAFT

Dwight L. Balough

March 1986

ABS The purpose of this report is to establish linear, decoupled models of rigid body motion for the fixed wing configuration of the Rotor Systems Research Aircraft. Longitudinal and lateral control surface fixed linear models were created from aircraft time histories using current system identification techniques. Models were obtained from computer simulation at 160 KCAS and 200 KCAS, and from flight data at 160 KCAS. Comparisons were performed to examine modeling accuracy, variation of dynamics with airspeed and correlation of simulation and flight data results. The results showed that the longitudinal and lateral linear models accurately predicted RSRA dynamics. The flight data results showed that no significant handling qualities problems were present in the RSRA fixed wing aircraft at the flight speed tested.

ABS Author